MATHEMATICAL MODELING OF HIGH AND LOW TEMPERATURE HEAT PIPES

By

S. W. Chi
Associate Research Professor

Final Report to Goddard Space Flight Center, NASA
Grant No. NGR 09-010-070

December 1971

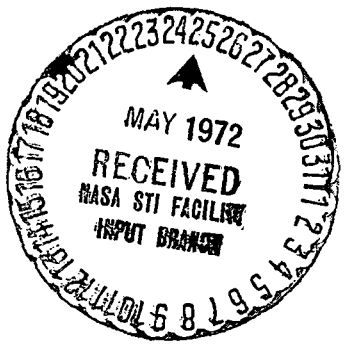

School of Engineering and Applied Science
The George Washington University
Washington, D.C. 20006

ABSTRACT

After a review of heat and mass transfer theory relevant to heat pipe performance, math models are developed for calculating heat-transfer limitations of high-temperature heat pipes and heat-transfer limitations and temperature gradient of low temperature heat pipes. Calculated results are compared with the available experimental data from various sources to increase confidence in the present math models.

For the convenience of the users of the present theory, complete listings of two computer programs for high- and low-temperature heat pipes respectively are appended to the report. These programs enables the performance of heat pipes with wrapped-screen, rectangular-groove or screen-covered rectangular-groove wick to be predicted.

LIST OF CONTENTS

NOMENCLATURE

a	half of groove width, Eq. (2.15)
A	cross-sectional area, Eq. (2.4)
B	a constant in Eq. (2.16)
C	permeability factor for capillary structure, Eq. (2.13)
c_f	frictional coefficient, Eq. (2.9)
c_{pf}	liquid specific heat at constant pressure, Eq. (2.28)
C_{sf}	correlation constant, Eq. (2.48)
De	effective diameter of capillary pores, Eq. (2.49)
Dg	diameter of vapor flow passage, Eq. (2.9)
F	coefficient for loss of dynamic pressure, Eq. (3.16)
g	gravitational acceleration, Eq. (2.2)
h	liquid rise in capillary tube, Eq. (2.2)
h_f	fully wetted liquid height in capillary groove, Eq. (2.6)
h_{fg}	heat of vaporization, Eq. (2.42)
K_e	effective thermal conductivity of liquid saturated wick, Eq. (2.24)
K_f	thermal conductivity of liquid, Eq. (2.24)
K_w	thermal conductivity of wick material, Eq. (2.24)
m_f	total liquid mass flow rate, Eq. (2.13)
m_l	liquid mass flow rate per groove, Eq. (2.20)
m'	liquid mass flow rate per unit length of evaporator or condenser, Fig. 2.6
$\dot{m}''$	vapor mass flow rate per unit of vapor flow area, Eq. (2.50)
$\dot{m}''_{max}$	maximum vapor mass flow rate per unit of vapor flow area, Eq. (2.59)

Nomenclature (continued)

M	Mach number, Eq. (2.54)
n	number of grooves, Eq. (3.19)
N_f	liquid transport factor, Eq. (3.6)
p_f	liquid pressure, Eq. (2.13)
p_g	vapor pressure, Eq. (2.9)
p_o	gas stagnation pressure, Eq. (2.51)
p_{vap}	vapor pressure, Eq. (2.44)
p_{liq}	liquid pressure, Eq. (2.44)
Δp_c	capillary pumping pressure, Eq. (2.1)
Δp_f	pressure drop due to liquid flow resistance, Eq. (3.1)
Δp_g	pressure drop due to vapor flow resistance, Eq. (3.15)
Δp_g	average pressure drop due to vapor flow resistance, Eq. (3.2
Δp_s	pressure drop due to gravitational force, Eq. (3.14)
P	wetted perimeter, Eq. (2.4)
q'	heat transfer rate per groove per unit length, Eq. (2.36)
q"	heat transfer rate per unit area, Eq. (2.48)
Q	heat transfer rate, Eq. (3.11)
Q_{max}	maximum heat transfer rate, Eq. (2.59)
r	radius, Eq. (2.3)
r_b	radius of vapor bubble, Eq. (2.24)
r_e	effective capillary radius for liquid flow, Eq. (2.13)
r_i	inner radius of heat pipes container, Fig. 2.1
r_g	radius of vapor flow passage, Fig. 2.1
r_1, r_2	principle radius of curvature of meniscus, Eq. (2.1)

Nomenclature (continued)

R	radius of capillary tube, Eq. (2.5)
R_E	equivalent radius of capillary structure, Eq. (2.8)
Re	Reynolds number based upon axial velocity and radius, Eq. (2.11)
Re_w	Reynolds number based upon radial velocity at tube wall and radius, Eq. (2.11)
t	thickness of wick structure, Eq. (3.3)
T	Temperature, Eq. (2.29)
T_c	condenser wall temperature, Eq. (3.30)
T_e	evaporator wall temperature, Eq. (2.30)
T_g	vapor temperature, Eq. (2.31)
ΔT_c	temperature difference defined as (Te-Tg), Eq. (2.40)
ΔT_e	temperature difference defined as (Tg-Tc), Eq. (3.30)
T_o	stagnation temperature, Eq. (2.52)
u	axial velocity, Eq. (2.9)
$\bar{u}$	bulk average axial velocity, Eq. (2.9)
v	radial velocity at tube wall, Eq. (2.11)
Wb	Weber number, Eq. (2.60)
x,y	co-ordinate axes, Eq. (2.29)
z	axial distance, Eq. (2.9)
z_a	length of adiabatic section, Eq. (3.4)
z_c	length of condenser, Eq. (3.4)
z_e	length of evaporator, Eq. (3.4)
z_t	total length of heat pipe, Eq. (3.3)

Nomenclature (continued)

α	defined as $(dp_f/dz)/\mu f$, Eq. (2.14)
γ	ratio of specific heats, Eq. (2.54)
δ	groove depth, Eq. (2.16)
ε	porosity of capillary structure, Eq. (2.24)
θ	wetting angle, Eq. (2.5)
μ_f	liquid dynamic viscosity, Eq. (2.13)
μ_g	vapor dynamic viscosity, Eq. (e.18)
ρ_f	liquid density, Eq. (2.13)
ρ_g	vapor density, Eq. (2.20)
ρ_o	gas density at stagnation state, Eq. (2.52)
σ	surface tension, Eq. (2.1)
τ_s	shear stress at tube wall, Eq. (2.9)
ϕ	nondimensional temperature, Eq. (2.31)
ψ	heat pipe elevation angle, Eq. (2.41)
ω	groove width, Eq. (2.22)

LIST OF FIGURES

I. INTRODUCTION

An Integrated Cryogenic Cooling Engine System[1] (ICICLE) currently under study at Goddard Space Flight Center is an attractive concept for providing long life cryogenic cooling space. Fig. 1.1 is a schematic illustration of the ICICLE System concept. A miniature Vuilleunier (VM) cycle cryogenic engine is the central cooling refrigerator. The engine has three temperature regions: a hot volume (≈900° K), an ambient temperature volume (≈310° K) and a cold volume (≈75° K). The VM engine operates on thermal power which is provided by a radioisotope. Because safety considerations will dictate the location of the isotope and experiment requirements will dictate the location of spaces which must be cooled, the components of the ICICLE System will be distributed on a spacecraft. Consequently, heat pipes ranging from cryogenic to liquid-metal temperatures are used to couple the VM engine to other components of the system.

An objective of this research is to develop math models for predicting performance of heat pipes of various wick structures (e.g. wrapped-screen, open-groove and screen-covered-groove wicks) and temperatures ranging from cryogenic to liquid-metal temperatures. As far as possible, the confidence in theoretical predictions will be established by comparison of theory with available experimental data.

Section II below is devoted to a review of heat and mass transfer theory leading to the development of present math models which is described in Section III. Also included in Section III are comparisons of present predictions with available experiments. For the convenience of users of the present math models two complete program listings for calculating performance of low- and high-temperature heat pipes respectively are appended to the report.

Conclusions and recommendations for further work are given in Section IV.

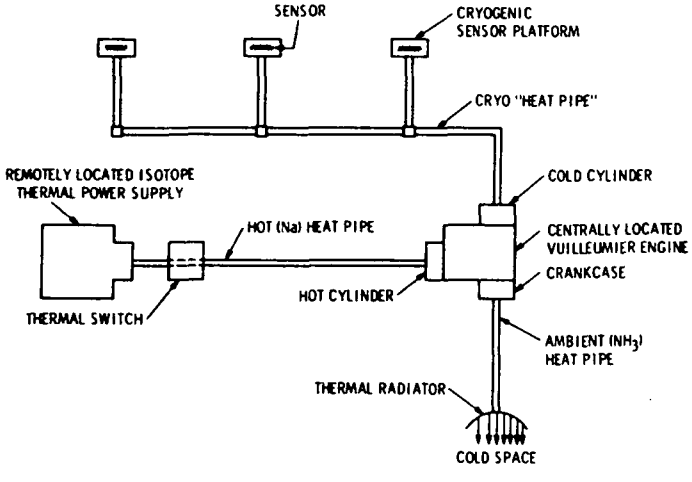

Figure 1.1 Schematic illustration of the ICICLE system concept

II. REVIEW OF HEAT AND MASS TRANSFER THEORY

1. Introductory Remarks

A well-known method for the transfer of a large amount of heat with small temperature drop consists of the evaporation of a liquid, transport of the vapor through a duct, and subsequent condensation. In order to work continuously, the condensate must be returned to the evaporator. Ordinarily this step is accomplished by gravity or by a pump. In a heat pipe[2] the return of liquid is accomplished by a wick of suitable capillary structure.

The principle of operation of a simple cylindrical heat pipe is shown schematically in Fig. 2.1. The wick is saturated with a wetting liquid. In the steady state the liquid temperature in the evaporator is maintained higher than in the condenser by an external heat source. The resulting difference in vapor pressure Δp_g drives vapor from the evaporator to condenser. The depletion of liquid by evaporation causes the vapor-liquid interface in the evaporator to retreat into the wick surface and a capillary pressure is developed. This capillary pressure pumps condensate back to the evaporator. The heat pipe can operate without drying out the wick as long as the capillary pressure term is greater than or equal to the sum of pressure drops due to liquid and vapor flow resistance and gravitational forces acting on the liquid.

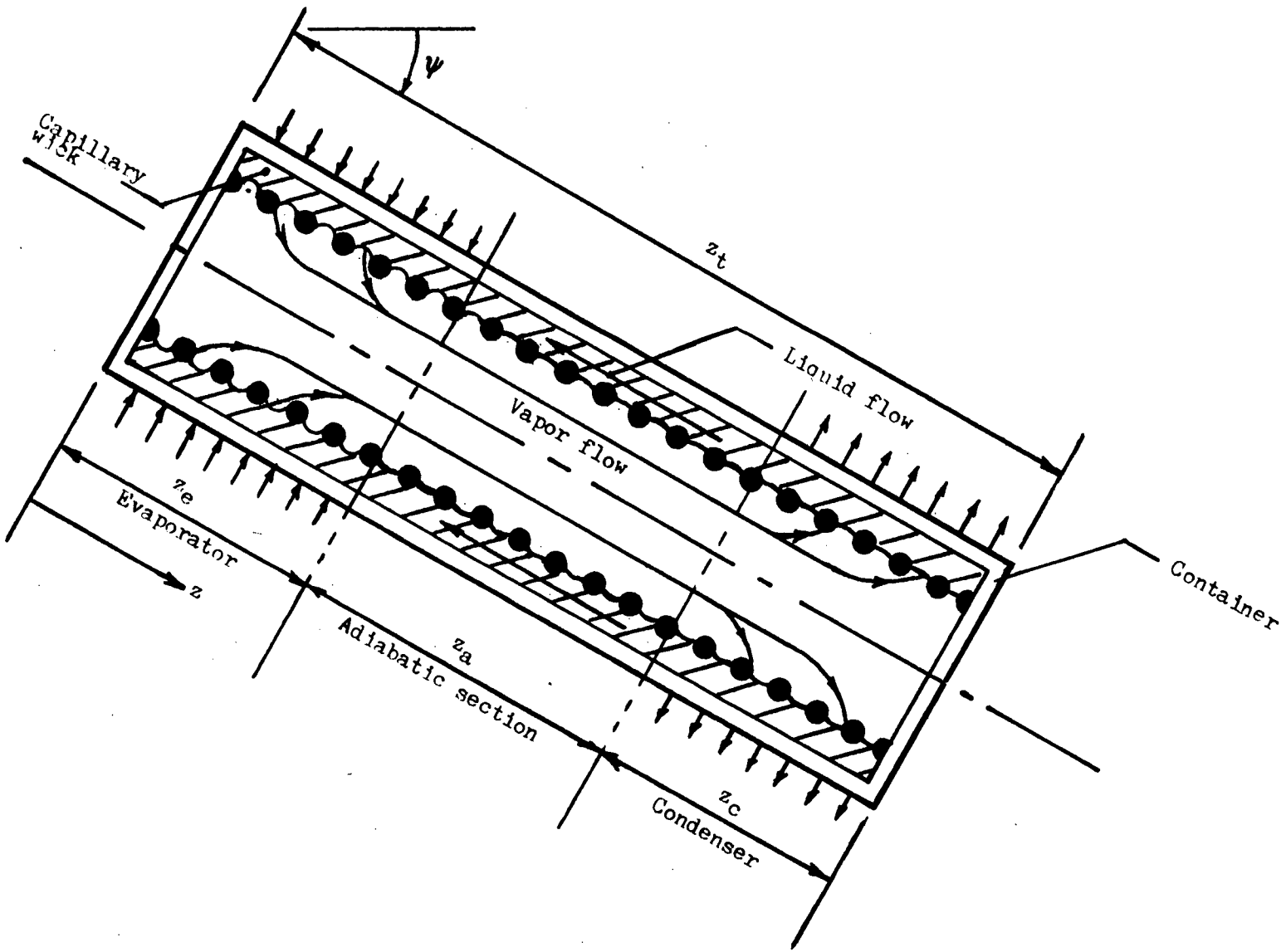

Figure 2.1 Schematic diagram of the principle of operation of a heat pipe

The temperature drop of a heat pipe equals to the sum of the temperature drops at the evaporator, vapor flow passage and condenser. Because of the usual thinness of wick structures and the small temperature drop at the vapor flow passages, the heat pipe exhibits a thermal conductance greatly in excess of that which could be obtained by the use of a homogeneous piece of any known metal.

However, unlike solid heat conductors, heat pipes cannot be characterized by a single property as equivalent thermal conductivity. Limitations and thermal conductance of a heat pipe are dependent upon not only the size, shape and materials of the heat pipe but also its heat transfer rate, wick structure and working fluid. Heat pipes using working fluids ranging from cryogens to liquid metals have been developed. Different types of wick structures have been used; several examples[3] are shown in Fig. 2.2. Heat and mass transfer theory relevant to heat pipe performance are reviewed below.

2. Capillary Pressure in Wick Structures

The well-known Laplace and Young equation for the capillary pressure difference, Δp_c, established at any point of a liquid vapor interface is

$$\Delta p_c = \sigma(1/r_1 + 1/r_2), \tag{2.1}$$

in which r_1 and r_2 are the principal radii of curvature of meniscus and σ the surface tension. The commonest method of measuring pressure differences across the meniscus in a

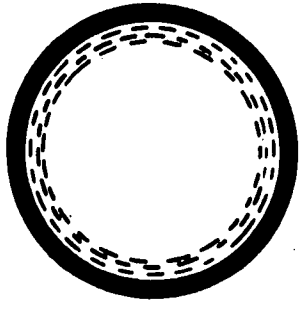

Wrapped screen

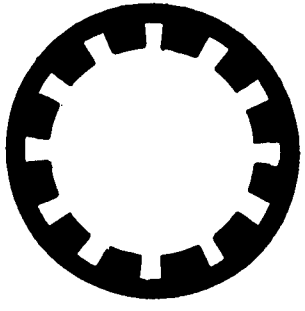

Open grooves

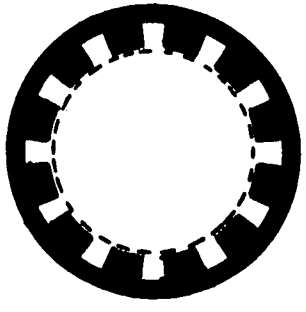

Screen covered grooves

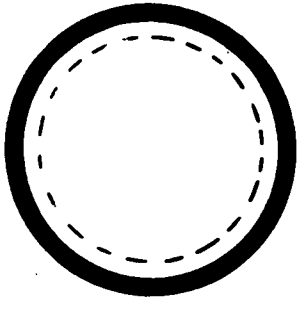

Annulus

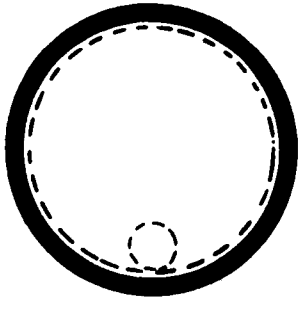

Artery

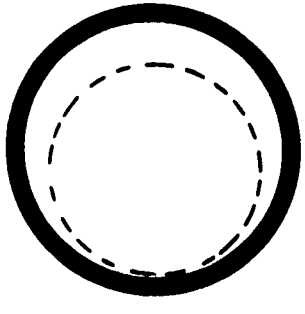

Crescent annulus

Figure 2.2 Cross section of various wick structures[3]

capillary is the observation of vertical liquid rise, h. Δp_c can then be related to h by the equation

$$\Delta p_c = (\rho_f - \rho_g) gh, \tag{2.2}$$

where ρ_f is the liquid density, ρ_g is the vapor density and g is the gravitational acceleration. For an approximate treatment of the capillary rise, when the radius of curvature of the meniscus is much smaller than the capillary rise, Eq. (2.1) can be reduced to a simpler relation with one radius of curvature, r, and the pressure-difference equation becomes

$$\Delta p_c = 2\sigma/r = (\rho_f - \rho_g) gh. \tag{2.3}$$

In the case of a perfectly wetting liquid in a capillary tube, the radius of curvature of the surface of the meniscus r approximates the hydraulic radius of the capillary, R, defined as

$$R = 2A/\mathcal{P}, \tag{2.4}$$

where A is the cross-sectional area and $\mathcal{P}$ the wetted perimeter. If the liquid, however, does not wet the capillary surface completely, an angle of contact between the liquid and the solid surface, θ, will be observed and the radius of curvature becomes $r = R \cos \theta$. Then, the capillary pressure differences and the vertical liquid rises can be accertained by the relation

$$\Delta p_c = (\rho_f - \rho_g) gh = 2\sigma \cos \theta/R. \tag{2.5}$$

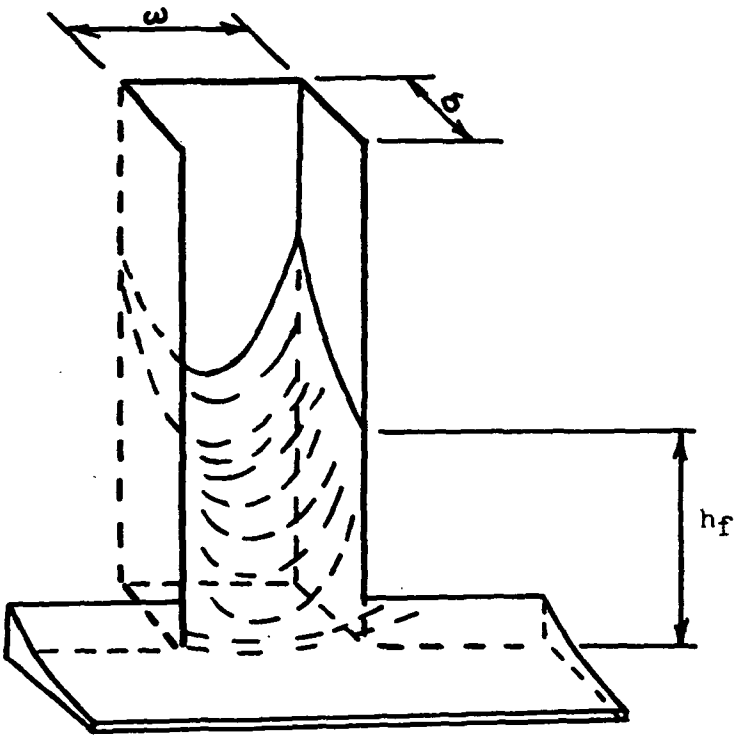

Figure 2.3 Liquid rise in a capillary groove

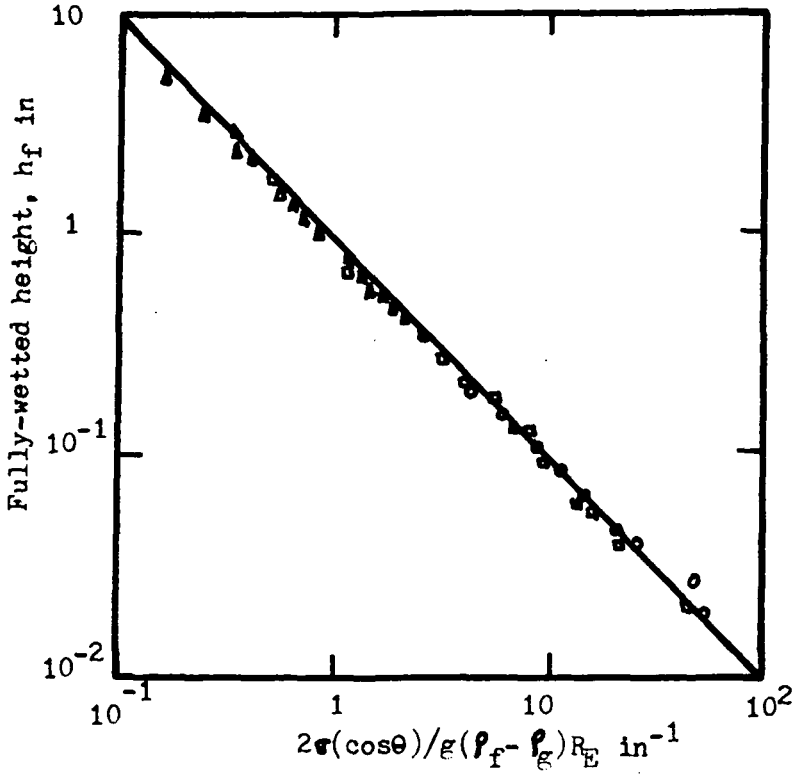

Figure 2.4 Calculated fully wetted liquid rise in capillary grooves[4]

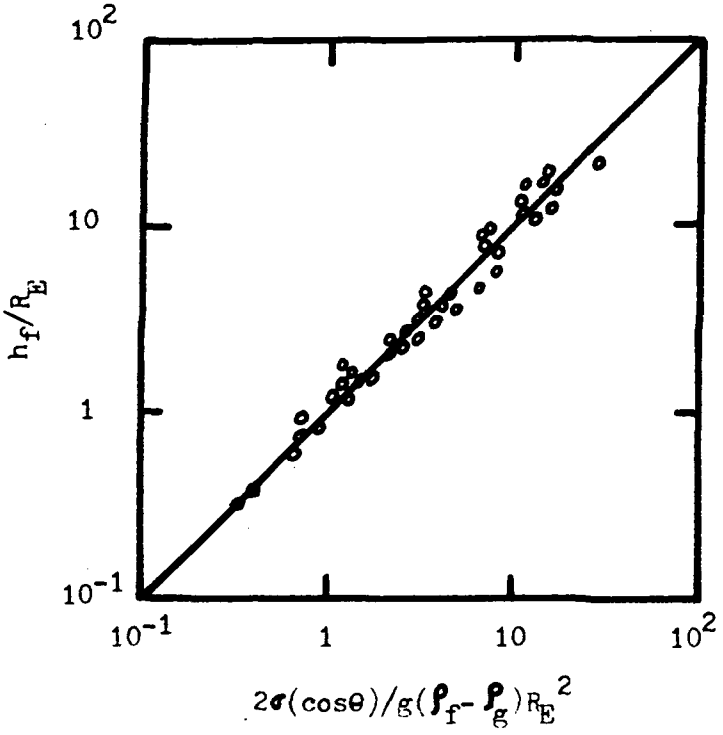

Figure 2.5 Measured dimensionless liquid rise in capillary grooves[4]

The liquid-vapor interface in a capillary groove under the action of gravity is shown schematically in Fig. 2.3. Experimental and theoretical studies of liquid interfaces in different shaped grooves have been made by Bressler and Wyatt[4]. It was found that both the measured and the calculated fully-wetted height can be represented accurately by a similar relation as given in Eq. (2.5)

$$\Delta p_c = (\rho_f - \rho_g) g h_f = 2\sigma \cos \theta / R \tag{2.6}$$

as shown in Figs. 2.4 and 2.5, when R for an open groove of cross-sectional area, A, wetted perimeter, $\wp$, and width, ω, is calculated by the equation

$$R = 2A/(\wp - \omega) \tag{2.7}$$

instead of Eq. (2.4).

Hence capillary pumping pressure, when $\rho_g << \rho_f$, can be calculated by the equation

$$\Delta p_c = 2\sigma \cos \theta / R_E \tag{2.8}$$

with R_E designated an equivalent radius defined as $2A/\wp$ for capillary tubes and $2A/(\wp - \omega)$ for open capillary grooves.

3. Vapor Pressure Drop

A stationary vapor control volume of diameter D_g and width dz with mass transfer per unit width m' is represented in Fig. 2.6 with the terms which appear in the momentum

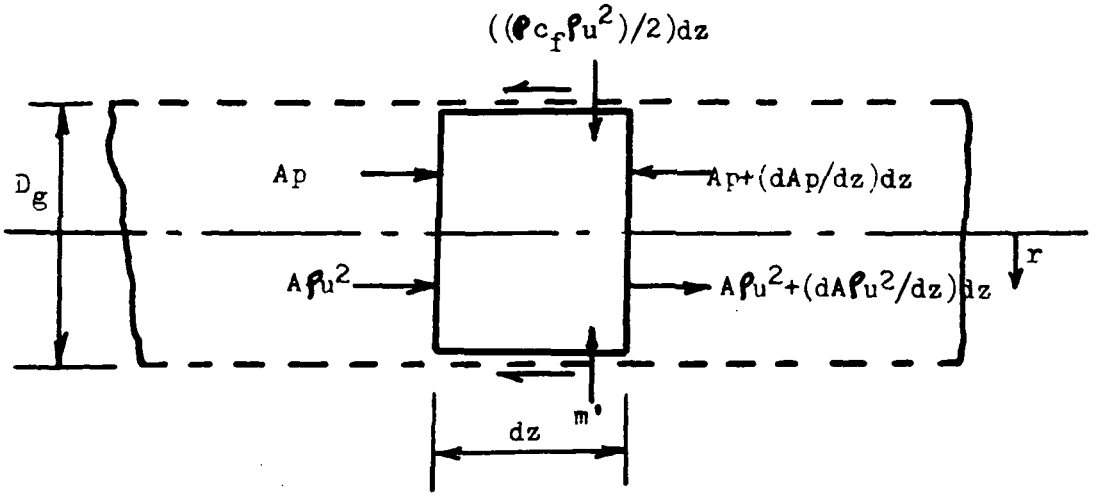

Figure 2.6 An elementary control volume for vapor flow

equation, where m' may be positive, zero or negative depending upon whether the evaporator, adiabatic section or condenser of a heat pipe is under consideration. The principle of conservation of axial momentum requires that

$$dp_g/dz = -2c_f\rho_g\bar{u}^2/D_g - 8(d\int_0^{D_g/2}\rho_g u^2 r dr/dz)/D_g^2,^* \qquad (2.9)$$

in which p_g is the vapor pressure, z is the axial distance, c_f is the skin friction coefficient $\tau_s/(\rho_g\bar{u}^2/2)$, Re is the Reynolds number $\rho_g\bar{u}D_g/\mu_g$, μ_g is the vapor dynamic viscosity, u is the vapor velocity, and $\bar{u}$ is the vapor bulk average velocity.

Integration of Eq. (2.9) from z = 0 to $z = z_t(=z_e+z_a+z_c)$ yields a relation for the total vapor pressure drop

$$\Delta p_g = \int_0^{z_t}(2c_f\rho_g\bar{u}^2/D_g)dz. \qquad (2.10)$$

It was noted in the above integration that u = 0 at both ends of a heat pipe. This Eq. (2.10) can be evaluated if the skin friction coefficient c_f is known.

The values of c_f for laminar flow may be obtained from numerical solution of complete Navier-Stokes equations for the tube flow with wall suction and injection. The dependence

---

*With negative m' axial momentum flux associated with m'(=m'u) may be subtracted from the righthand side of Eq. (2.9); but for heat pipe application condensation occurs at the vicinity of the liquid-vapor interface where u is small, so it is neglected in the present analysis.

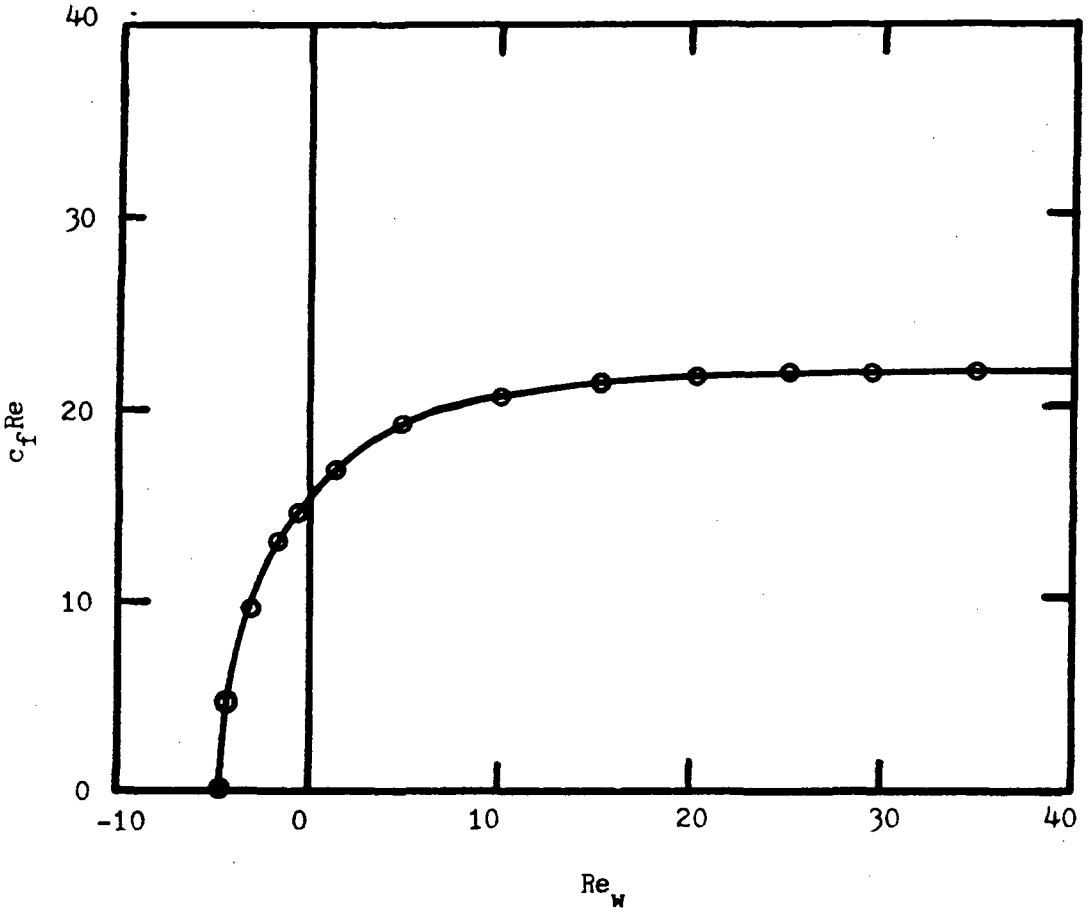

Figure 2.7 Friction coefficient for the fully developed flow. o, exact numerical solution; _____, empirical Eq. (1.11).

of the fully developed $c_f Re$ on the wall Reynolds number $Re_w (=\rho_g v D_g/\mu_g)$ from Yuan and Finkelstein's solution[5,6] is shown in Fig. 2.7. It can be seen in this figure that the empirical equation

$$c_f Re = 1/[0.048 + 0.0494/(4.7 + Re_w)^{0.8}], \tag{2.11}$$

accurately represents the exact numerical data for negative as well as positive Re_w. It can also be seen in this figure that at $Re_w = 0$ Eq. (2.11) reduces to

$$c_f Re = 16/Re, \tag{2.12}$$

which is the well-known Hagen-Poiseuille solution for the fully developed tube flow without wall mass flux.

It should be noted that in the above derivation of Eq. (2.10) for the vapor-pressure drop complete recovery of dynamic pressure due to vapor velocity has been assumed. However, it can be seen in Fig. 2.7 that the friction coefficient c_f, and therefore the velocity gradient at the wall also, becomes zero at $Re_w = -4.5978$. At further increase in suction, negative velocity gradient exists at the wall; a and reverse flow is likely to occur. When the flow reverse occurs, the recovery of dynamic pressure becomes difficult[7]. Unfortunately, no quantitative information is available at the present time to account for the loss of dynamic pressure at reverse flows. This information is urgently needed, because most heat pipes have large $/Re_w/$ values at the condenser.

4. Liquid Pressure Drop

For the flow of liquid through capillary structures, the liquid pressure gradient in the axial direction dp_f/dz may be calculated by the equation[2],

$$dp_f/dz = c\mu_f m_f/(Ar_e^2\rho_f), \tag{2.13}$$

where c is a dimensionless constant depending on the detailed geometry of the capillary structure, μ_f is the liquid dynamic viscosity, m_f is the liquid mass flow rate, A is the total cross-sectional area for liquid flow, r_e is the effective hydraulic radius for liquid flow , and ρ_f is the liquid density. For non-connected parallel circular cylinder c = 8, and for concentric annular c = 12. However, for wrapped screen the value of c is uncertain and dependent upon the screen mesh size and the wrapping tightness.

For liquid flow in passages of simple geometry such as those of open and closed grooves shown in Figs. 2.8, expressions for the pressure drop may be derived by theoretical consideration. The governing equation for the fully developed laminar flow of liquid in grooves can be written as

$$\partial^2 u/\partial x^2 + \partial^2 u/\partial y^2 = \alpha, \tag{2.14}$$

where α is defined as $(dp_f/dz)/\mu_f$. Eq. (2.14) can be solved with appropriate boundary conditions. For example, for flow

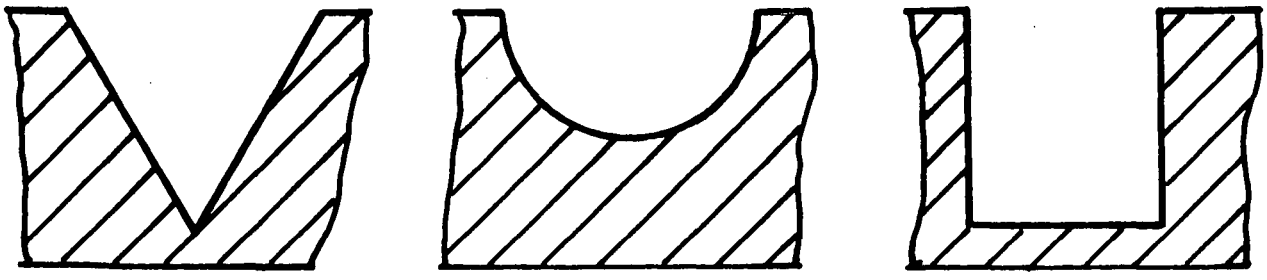

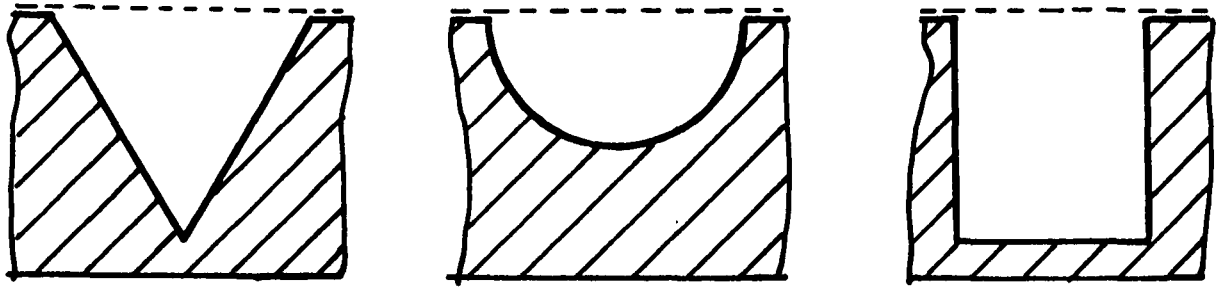

Figure 2.8 Cross section of various open and screen-covered grooves

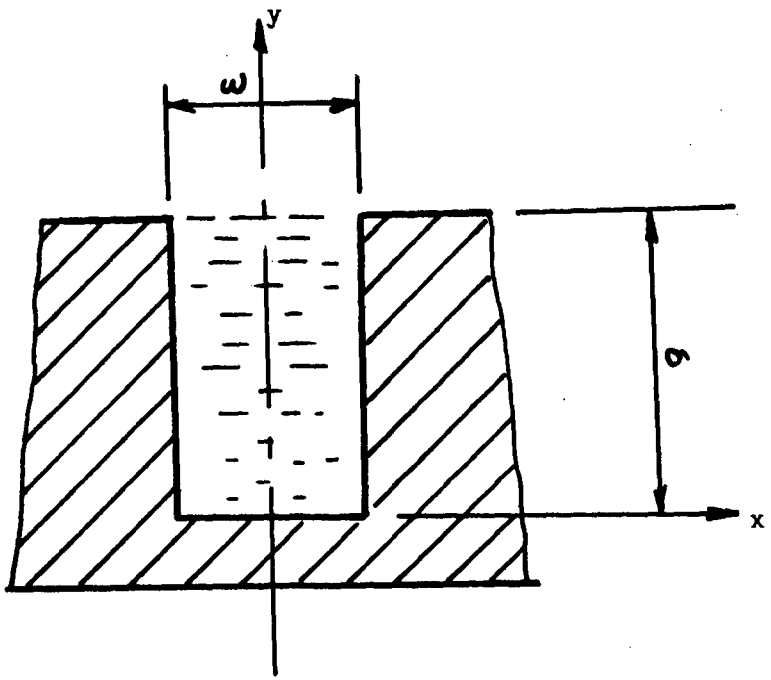

Figure 2.9 Co-ordinate system for liquid flow analysis

in an open rectangular groove of Fig. 2.9 the boundary conditions are:

$$u = 0, \text{ @ } x = \pm a \text{ \& } y = 0; \text{ and } \partial u/\partial y = 0, \text{ @ } y = \delta; \tag{2.15}$$

and solution of Eq. (2.14) may be sought in the form

$$u = B(a^2 - x^2)y\ (\delta - y/2) \tag{2.16}$$

which satisfies the boundary conditions (2.15). In accordance with the method of Galerkin[8], we obtain for determination of B the equation

$$\int_{x=0}^{a} \int_{y=0}^{\delta} (\partial^2 u/\partial x^2 + \partial^2 u/\partial y^2 - \alpha)(a^2 - x^2)y(\delta - y/2)\,dxdy = 0. \tag{2.17}$$

whence

$$B = 5\alpha/[4(a^2 + \delta^2)] \tag{2.18}$$

and the required solution is

$$u = -5\alpha(a^2 - x^2)y(\delta - y/2)/[4(a^2 + \delta^2)]. \tag{2.19}$$

Now mass flow rate in each groove m_1 may be determined by the equation

$$m_1 = 2 \int_{x=0}^{a} \int_{y=0}^{\delta} \rho_f u\,dxdy. \tag{2.20}$$

On substitution of u from Eq. (2.19) into the above Eq. (2.20) there is obtained

$$m_l = -5\rho_f \alpha a^3 \delta^3 / 9(a^2+\delta^2) \tag{2.21}$$

or

$$dp_f/dz = -18(\omega^2+4\delta^2)\mu_f m_l/(5\omega^3\delta^3\rho_f), \tag{2.22}$$

for the liquid pressure drop in an open groove of depth δ and width ω.

If similar analysis is made for liquid flows in covered grooves of depth δ and width ω, the resultant expression for the pressure gradient will be

$$dp_f/dz = -72(\omega^2+\delta^2)\mu_f m_l/(5\omega^3\delta^3\rho_f). \tag{2.23}$$

5. Heat Transfer

The primary heat-transfer mechanism for heat pipes is thermal conduction through the liquid saturated wick with surface evaporation at the evaporator section and film condensation with conduction through the liquid-saturated wick at the condenser section. Values of the thermal conductivity of heterogeneous materials such as the liquid-saturated wick are dealt with by Gorring and Churchill[9].

The simplest configurations, as shown in Fig. 2.10, consist of arrangement of wick material and liquid in series or parallel. The exact solutions for these cases are respectively,

$$K_e = K_f K_w / [\varepsilon K_w + K_f(1-\varepsilon)] \tag{2.24}$$

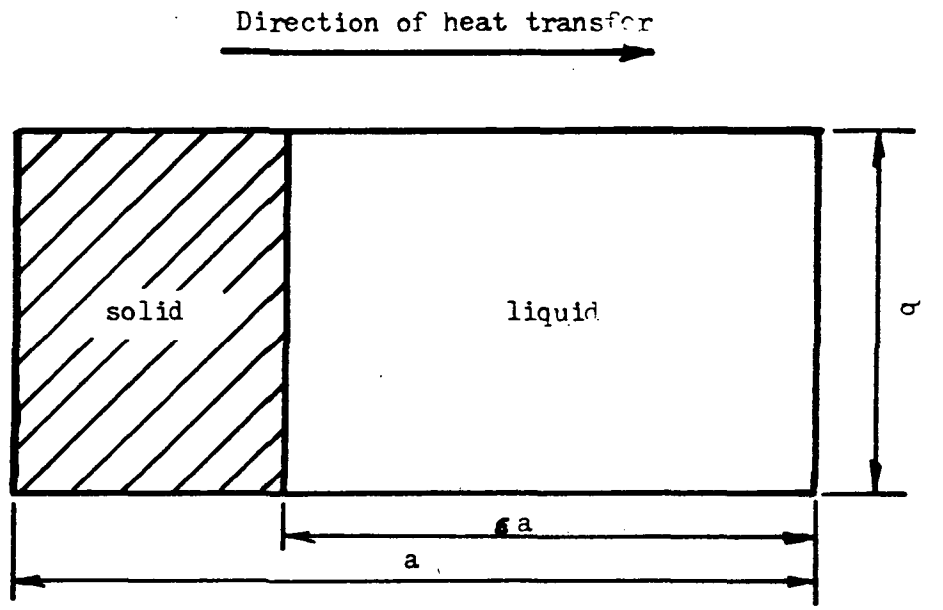

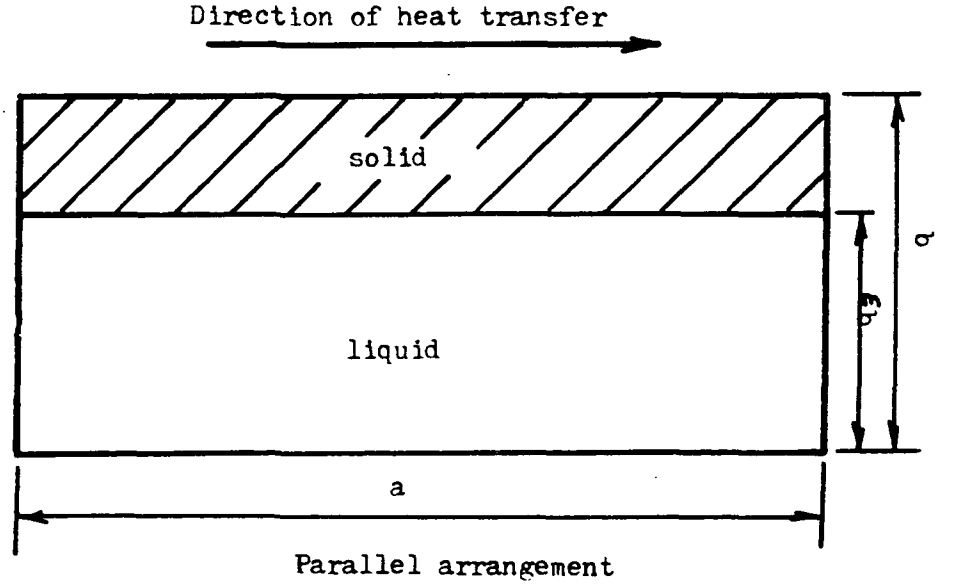

Figure 2.10 Heat transfer model for series or parallel arrangement of liquid-saturated wick structures

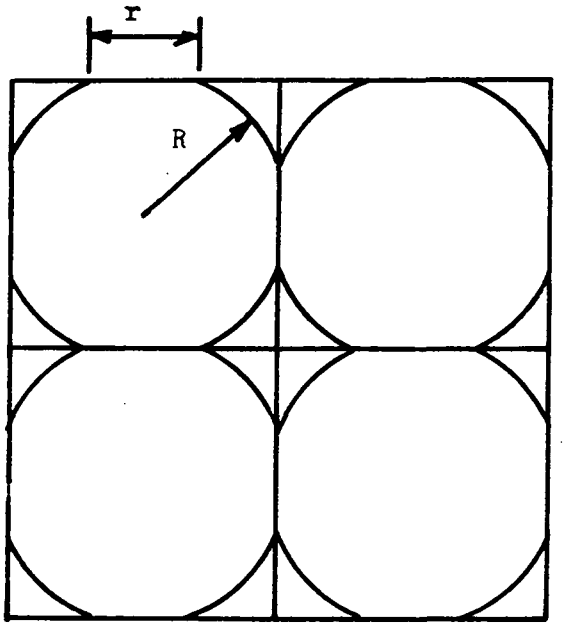

Figure 2.11 Heat transfer model for cubic array of truncated spheres

and

$$K_e = \varepsilon K_f + (1-\varepsilon)K_w \tag{2.25}$$

in which ε is the volume fraction of liquid, K_e is the thermal conductivity of the liquid saturated wick, K_f is the thermal conductivity of the liquid, and K_w is the thermal conductivity of the wick material. Thermal conductivities for the liquid saturated wick of distributed cylinders and spheres can be calculated respectively by the equations

$$K_e = K_f[K_f+K_w -(1-\varepsilon)(K_f-K_w)]/[K_f+K_w+(1-\varepsilon)(K_f-K_w)], \tag{2.26}$$

and

$$K_e = K_f[2K_f+K_w -2(1-\varepsilon)(K_f-K_w)]/[2K_f+K_w+(1-\varepsilon)(K_f-K_w)]. \tag{2.27}$$

The thermal conductivity of a simple cubic array of adjoined, truncated spheres having circles of contact of radius r as illustrated in Fig. 2.11 is as follows:

$$K_e = K_w/[(R/r) + (\ln 2R/r)/\pi], \tag{2.28}$$

when fluid surrounding the array is postulated to have zero conductivity and the radius of contact was assumed to be small relative to the radius of the spheres.

For some simple geometries, analytical expression for film evaporation and condensation can be derived in a straightforward manner. For example, for the case of film evaporation from rectangular grooved wick as shown in Fig. 2.12 with $K_f << K_w$

if liquid depletion is neglected, the conduction equation for the liquid in grooves may be written as:

$$\partial^2 T/\partial x^2 + \partial^2 T/\partial y^2 = 0, \tag{2.29}$$

and the approximate boundary conditions may be written as:

$$@\ x = 0,\ x = \omega\ \&\ y = 0:\quad T = \text{evaporator wall temperature, } T_e;$$

$$@\ y = \delta:\quad T = \text{vapor temperature, } T_g. \tag{2.30}$$

On the introduction of ϕ defined as:

$$\phi = (T-T_e)/(T_g-T_e), \tag{2.31}$$

Eq. (2.31) becomes

$$\partial^2 \phi/\partial x^2 + \partial^2 \phi/\partial y^2 = 0 \tag{2.32}$$

with boundary conditions

$$@\ x = 0,\ x = \omega\ \&\ y = 0:\ \phi = 0;\ \text{and}\ @\ y = \delta:\ \phi = 1. \tag{2.33}$$

A solution of Eq. (2.32) with boundary conditions (2.33) by the separation-of-variables method is:

$$\phi = (2/\pi) \sum_{n=1}^{\infty} \{[(-1)^{n+1} + 1]/n\} \sin(n\pi x/\omega) \sinh(n\pi y/\omega)/\sinh(n\pi\delta/\omega) \tag{2.34}$$

Hence the temperature of the liquid is given by the equation

$$T = T_e + (T_g-T_e)(2/\pi) \sum_{n=1}^{\infty} \{[(-1)^n+1]/n\} \sin(n\pi x/\omega) \sinh(n\pi y/\omega) /\sinh(n\pi\delta/n). \tag{2.35}$$

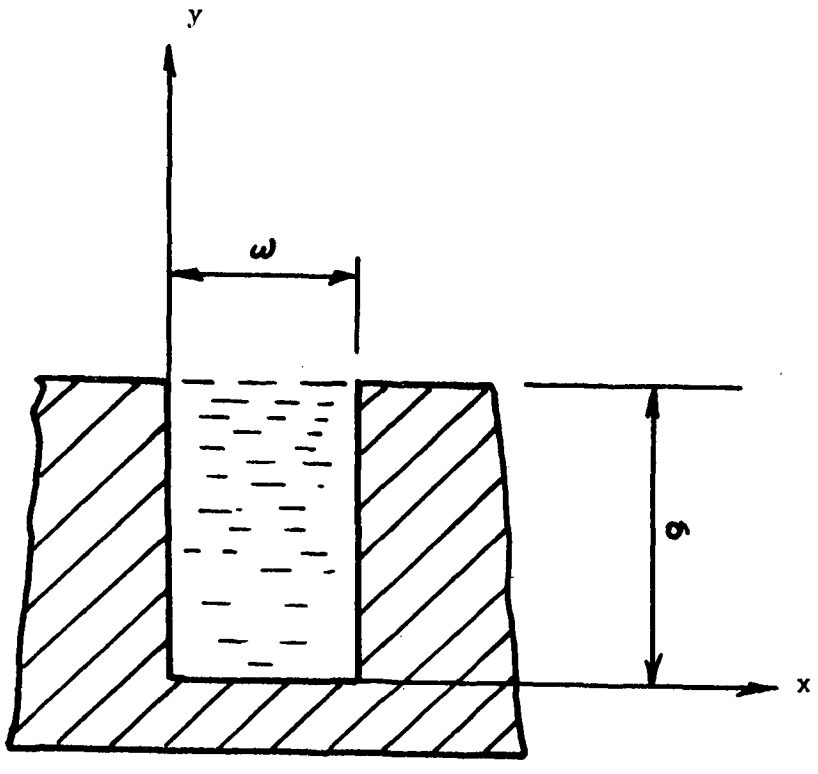

Figure 2.12 Co-ordinate system for analysis of heat transfer in rectangular grooves

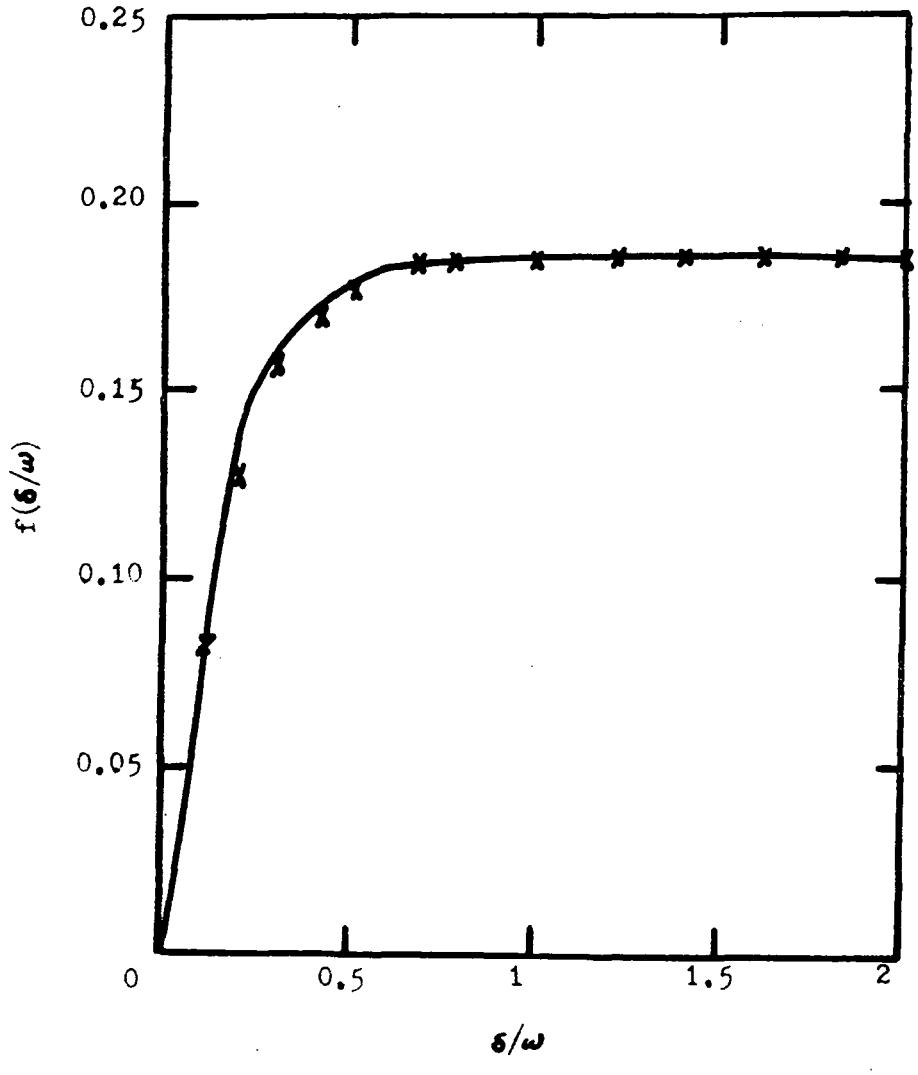

Figure 2.13 $f(\delta/\omega)$ versus (δ/ω). x, exact $f(\delta/\omega)$ Eq. (1.38); ——, approximate $f(\delta/\omega)$ Eq. (1.39).

The heat transfer per unit length of the rectangular groove q' can then be calcullated by the equation:

$$q' = -2K_f \int_0^{\omega/2} (\partial T/\partial y)_{y=0}\, dx, \tag{2.36}$$

that is

$$(T_e - T_g) = q'/\{K_f(4/\pi) \sum_{n=0}^{\infty} [2/(2m+1)]\coth[(2m+1)\pi\delta/\omega]\}. \tag{2.37}$$

Now let

$$f(\delta/\omega) \equiv \pi/\{4 \sum_{m=0}^{\infty} [(2/(2m+1)\coth((2m+1)\pi\delta/\omega)]\}. \tag{2.38}$$

Fig. 2.13 shows that the exact values of $f(\delta/\omega)$ can be represented accurately by the equation

$$f(\delta/\omega) = 0.185\ \text{th}[5.4(\delta/\omega)]. \tag{2.39}$$

Hence the evaporator temperature drop for the rectangular grooved wick with $K_f << K_w$ can be calculated accurately by the equation

$$\Delta T_e = 0.185\ q'\{\text{th}[5.4(\delta/\omega)]\}/K_f. \tag{2.40}$$

6. Miscellaneous Topics

(i) Gravitational force. The pressure drop due to gravity Δp_s in a column of liquid as shown in Fig. 2.14 can be calculated simply by the equation

$$\Delta p_s = \rho_f g z_t \sin\psi, \tag{2.41}$$

where Δp_s is defined as $(p_2 - p_1)$ and g is the gravitational acceleration.

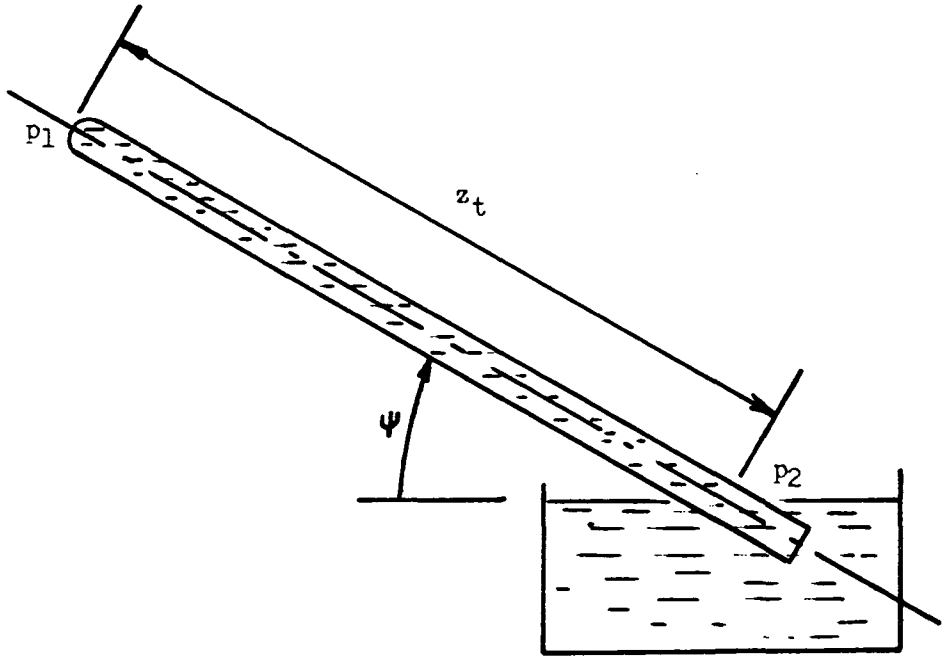

Figure 2.14 Pressure drop due to gravitational force, $\Delta P_s = P_2 - P_1$

(ii) Vapor temperature drop. The Clausius-Clapeyron equation with the perfect gas approximation relates T_g and p_g along the saturation line

$$dp_g/dT_g = h_{fg}\rho_g/T_g \tag{2.42}$$

where h_{fg} is the heat of vaporization. Hence the vapor temperature drop ΔT_g is related to the vapor pressure drop Δp_g by the equation

$$\Delta T_g = T_g \Delta p_g/(\rho_g h_{fg}). \tag{2.43}$$

(iii) Nucleate boiling. Imagine a spherical vapor bubble of radius r_b in a liquid; at equilibrium

$$\pi r_b^2 (p_{vap} - p_{liq}) = 2\pi r_b \sigma. \tag{2.44}$$

For heat pipe application p_{vap} corresponds to the saturation vapor pressure at the evaporator wall temperature T_e and p_{liq} corresponds to the pressure of the vapor at the evaporator p_g Eq. (2.44) can be written as

$$p_e - p_g = 2\sigma/r_b. \tag{2.45}$$

Since $(p_e-p_g) \simeq (T_e-T_g)(dp/dT)$, we can combine Eqs. (2.42) and (2.45) to get

$$T_e-T_g = 2T_g\sigma/(h_{fg}\rho_g r_b). \tag{2.46}$$

Hence if

$$T_e-T_g > 2T_g\,\sigma/(h_{fg}\rho_g r_b). \tag{2.47}$$

a bubble of radius r_b will grow and nucleate boiling may occur.

A large number of experimental data for nucleation boiling have been reported; and a number of correlation equations for empirical data have been derived. Rohsenow[10] reports the following correlation equation which satisfactorily represents the pool nucleate boiling data of a number of investigators:

$$c_{pf}(T_e-T_g)/h_{fg} = C_{sf}\{[\dot{q}"/(\mu h_{fg})\sqrt{\sigma/[g(\rho_f-\rho_g)]}\}^{1/3}(\mu_f c_{pf}/K_f) \tag{2.48}$$

in which c_{pf} is the liquid specific heat, $\dot{q}"$ is the heat flux density, and C_{sf} is the correlation constant ranging from 0.002 to 0.015 dependent upon surface-fluid combinations. For example, for water-platinum combination c_{gf} = 0.013 and for water-nickel C_{sf} = 0.006.

Allingham and McEntire[11], made both theoretical and experimental studies of nucleate boiling from water-saturated wick material. They recommend the following correlation equation:

$$\dot{q}"/[c_{pf}G(T_e-T_g)] = 0.072(c_{pf}\mu_f/K_f)^{-0.6}(\rho_f\sigma/p_g^2)^{-0.21}(D_eG/\mu_f)^{-0.77}, \tag{2.49}$$

where G is defined as $\dot{q}''/\varepsilon h_{fg}$, ε is the wick porosity and D_e is the effective diameter of the capillary pores.

(iv) Sonic velocity. For gas flow with wall injection and suction as shown in Fig. 2.15, the maximum axial mass flux density $\dot{m}''$ occurs at the downstream end of the injection section. On consideration of a control volume for the injection section, the conservation of mass, momentum and energy requires that

$$\dot{m}'' = \rho u, \tag{2.50}$$

$$p_o = p + \rho u^2, \tag{2.51}$$

$$T_o = T + u^2/(2C_p); \tag{2.52}$$

and the ideal gas law states that

$$p_o/(\rho_o T_o) = p/(\rho T). \tag{2.53}$$

In the above Eqs. subscript o indicates stagnation state of the injected gas. In terms of Mach number M, Eqs. (2.50) through (2.52) may be rewritten as:

$$\dot{m}'' = \rho M\sqrt{\gamma RT}, \tag{2.54}$$

$$p_o/p = 1 + \gamma M^2, \tag{2.55}$$

$$T_o/T = 1 + (\gamma-1)M^2/2. \tag{2.56}$$

In the above Eqs. γ is the ratio of specific heats, and R is the gas constant. Combination of Eqs. (2.53) and (2.55) and (2.56) yields an expression for the density ratio

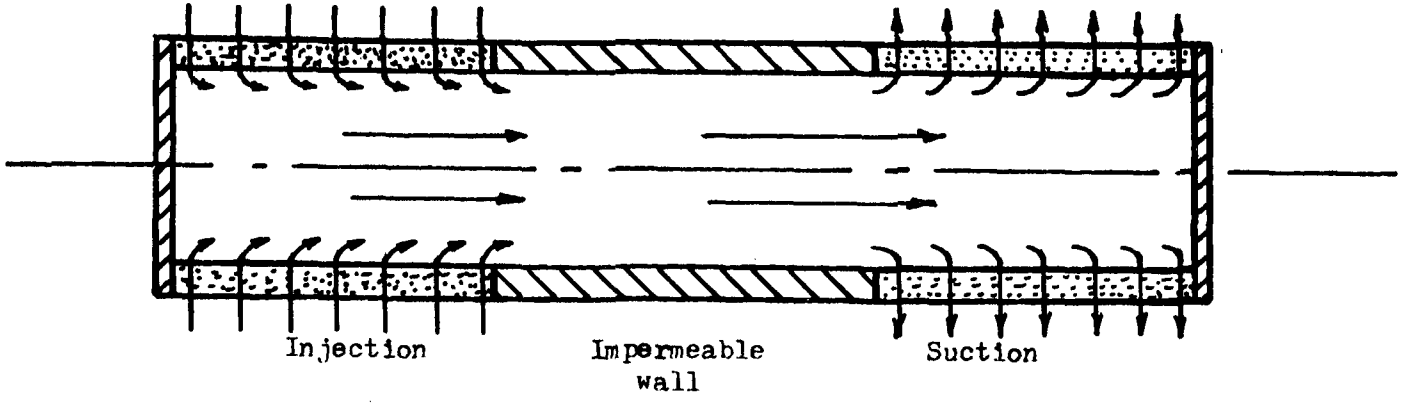

Figure 2.15 Schematic diagram of tube flow with wall injection and suction

$$\rho_o/\rho = (1+\gamma M^2)/[1+(\gamma-1)M^2/2]. \tag{2.57}$$

From Eqs. (2.54), (2.56) and (2.57), the following expression for $\dot{m}''$ can be derived

$$\dot{m}'' = \rho_o\sqrt{\gamma RT_o}\, M[1+(\gamma-1)M^2/2]^{1/2}/(1+\gamma M^2). \tag{2.58}$$

The maximum mass flux density possible $\dot{m}''_{max}$ for a given stagnation condition is at M equal to unity. $\dot{m}''_{max}$ can therefore be calculated by Fig. (2.58) with M = 1, i.e.

$$\dot{m}''_{max} = \rho_o\sqrt{\gamma RT_o/[2(\gamma+1)]} \tag{2.59}$$

(V) Entrainment. For a vapor flow over a liquid surface, the force which tends to tear the liquid apart is proportional to the product of dynamic pressure $\rho_g\bar{u}^2/2$ and square of a characteristic length a^2, and the force which holds the surface liquid is proportional to the product of surface tension of the liquid σ and a characteristic length a. At high velocity, some liquid may be entrained by the vapor. Weber number Wb defined as the ratio of the two forces mentioned above, namely:

$$Wb \equiv \rho_g u^{-2} a/\sigma, \tag{2.60}$$

is used as a criterion for the liquid entrainment.

III. PERFORMANCE OF HEAT PIPES

Performance of a heat pipe is dependent upon the properties of its working fluid. An approximate analysis of heat pipes with various working fluids will first be made below and then mathematical models for steady operation of low-temperature as well as high-temperature heat pipes will be developed.

1. Approximate Analysis

For qualitative comparison of heat-pipe performance with various working fluids, an approximate theory is to be developed for a simple cylindrical heat pipe at horizontal orientation as shown in Fig. 3.1. The following simplifying assumptions are made:

(i) Liquid wets the wick completely,

(ii) Vapor pressure losses are negligible,

(iii) Wick thickness t is much smaller than the radius of the vapor flow passage,

(iv) Heat flux density is uniform at the evaporator and condenser surface,

(v) Thermal conductivity of the liquid-saturated wick is proportional to that of the liquid.

The pressure balance for steady operation of this heat pipe can then be written

$$\Delta p_c = \Delta p_f. \tag{3.1}$$

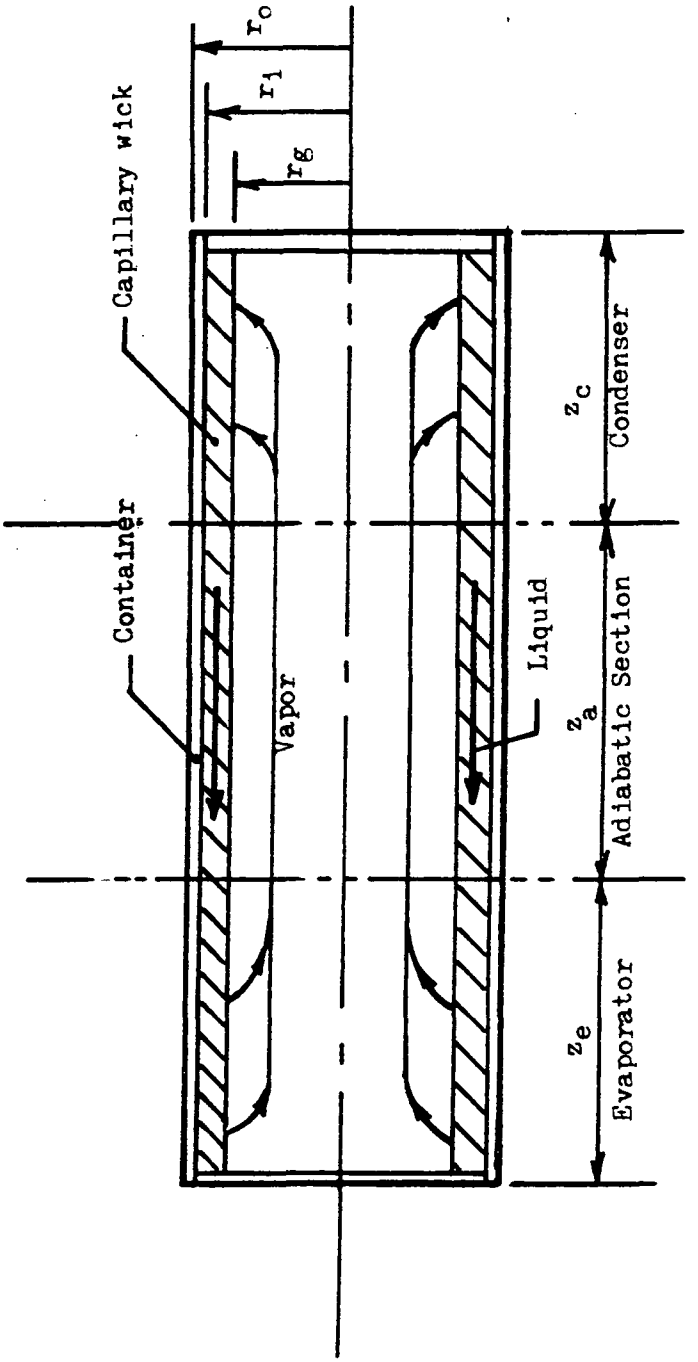

Figure 3.1 Schematic diagram of a cylindrical heat pipe at horizontal orientation

At the maximum heat flux Q_{max}, capillary pressure Δp_c can be evaluated by Eq. (2.8) with $\theta = 0$, i.e.

$$\Delta p_c \approx 2\sigma/R_E \tag{3.2}$$

and liquid pressure drop due to flow resistance Δp_f can be evaluated approximately by integrating Eq. (2.13), namely:

$$\Delta p_f \approx \int_0^{z_t} [c\mu_f m_f/(2\pi t r_i r_e^2 \rho_f \varepsilon)]dz. \tag{3.3}$$

In this Eq. (3.3) the axial distribution of m_f in terms of Q_{max} can be written as:

$$\begin{aligned} &@\ 0 \le z \le z_e: && m_f = Q_{max}\, z/(z_e h_{fg}) \\ &@\ z_e \le z \le (z_e+z_a): && m_f = Q_{max}/h_{fg} \\ &@\ (z_e+z_a) \le z \le z_t: && m_f = Q_{max}\,\{1-[z-(z_e+z_a)]/z_e\}/h_{fg} \end{aligned} \tag{3.4}$$

Substitution from Eq. (3.4) followed by integration results in the following expression for Δp_f:

$$\Delta p_f = cQ_{max}\mu_f(z_e+2z_a+z_c)/(4\rho_f h_{fg}\pi r_i r_e^2 t\varepsilon). \tag{3.5}$$

Combination of Eqs. (3.2) and (3.5) yields an expression for Q_{max}:

$$Q_{max} = N_f t\{8\pi r_i r_e^2 \varepsilon/[cR_E(z_e+2z_a+z_c)]\}. \tag{3.6}$$

Where N_f is the liquid transport factor defined as $\sigma\rho_f h_{fg}/\mu_f$, and it is a function of the working-fluid properties. All other terms on the right hand side of Eq. (3.5) depend on the heat pipe design. Fig. 3.2 shows the values of the liquid transport factor, N_f, for several heat-pipe working fluids.

The temperature gradient of a heat pipe is determined by the heat flux density and the radial thermal conductance of the wick material saturated with the working fluid in the liquid state. Based upon the simplifying assumptions (iii) and (v) described above, the conductance of the liquid-saturated wick U is seen to be proportional to the thermal conductivity of the liquid divided by the wick thickness, i.e.,

$$U \propto K_f/t \quad \text{or} \quad \Delta T \propto Qt/K_f. \tag{3.7}$$

Now for a heat pipe of fixed physical dimensions, its approximate operating characteristics with different working fluid may be derived from Eqs. (3.6) and (3.7). These are: (a) the maximum heat-transfer capability of the heat pipe is directly proportional to the values of liquid transport factor of the working fluid, and (b) the temperature drop at equal heat-transfer rate is inversely proportional to the liquid thermal conductivity of the working fluid. Fig. 3.3 shows the values of the liquid thermal conductivity for several fluids.

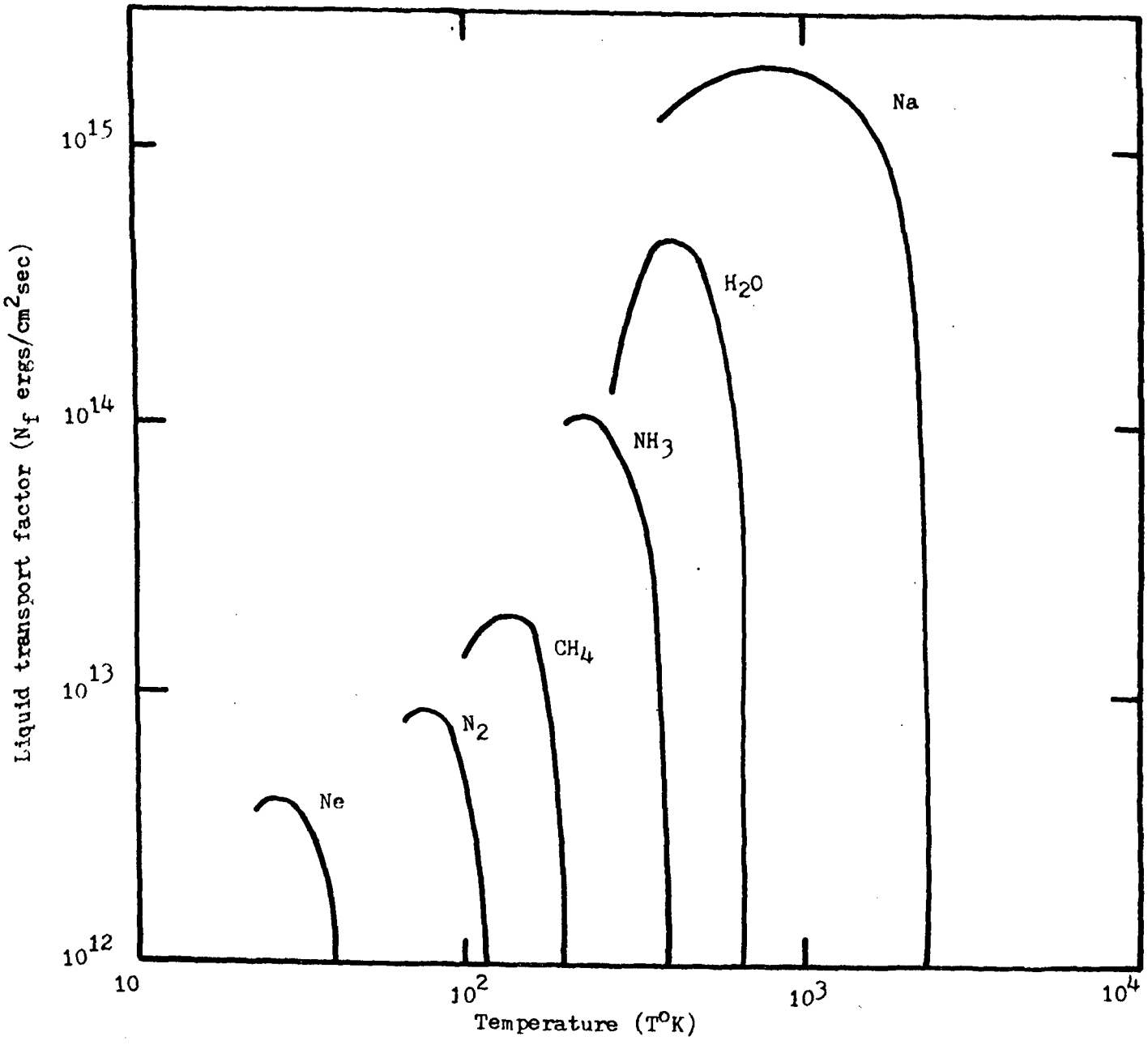

Figure 3.2 Liquid transport factor of several heat-pipe working fluid

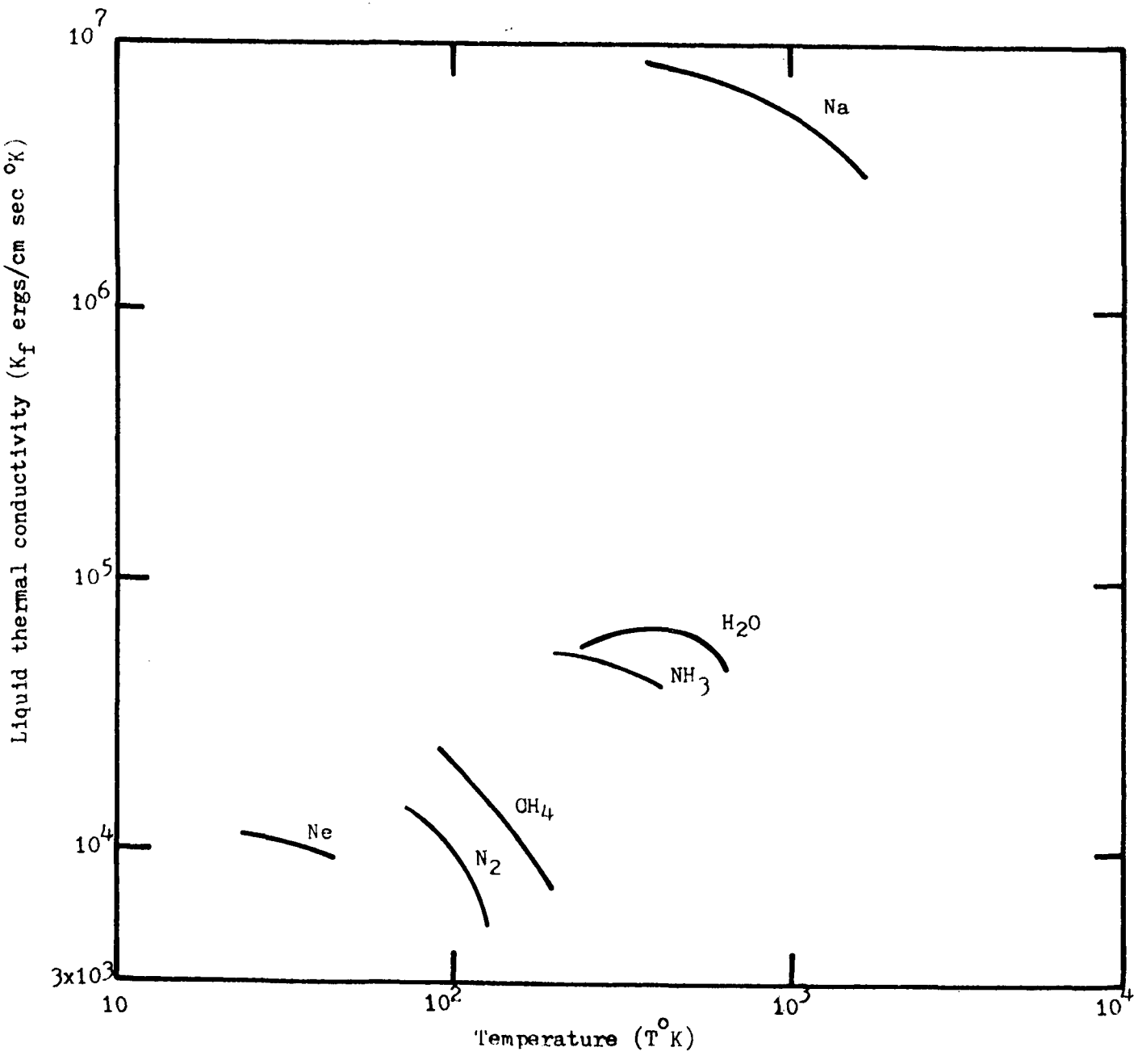

Figure 3.3 Liquid thermal conductivity of several heat-pipe working fluids

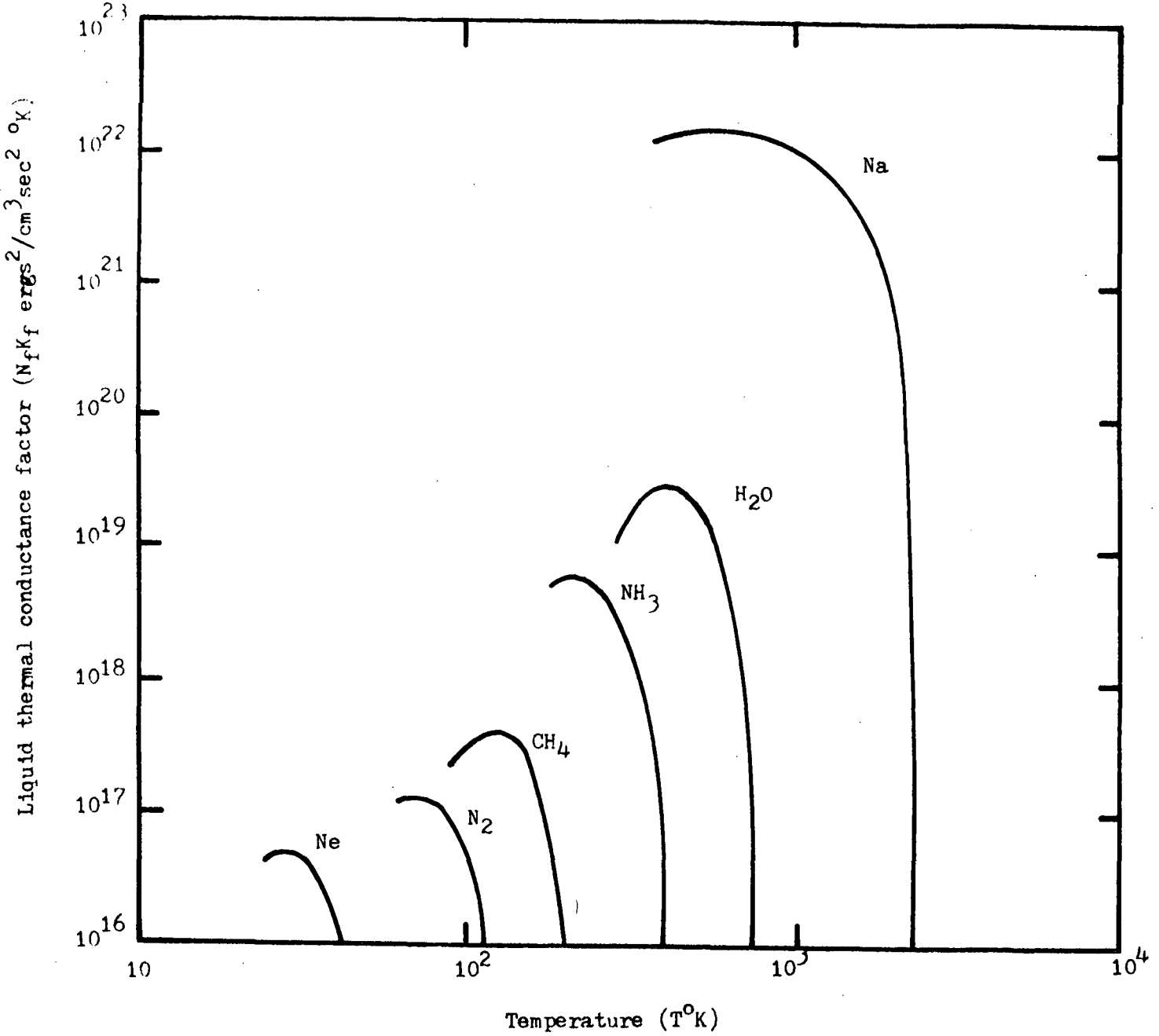

Figure 3.4 Liquid thermal conductance factor of several heat pipe working fluids

Similarly, the approximate operating characteristics of heat pipes of equal maximum heat transfer capability may also be derived from Eqs. 3.6 and 3.7. These are: (a) the wick thickness required is inversely proportional to the value of the liquid transport factor of the working fluid; and (b) the temperature drop at equal heat transfer rate is inversely proportional to the product of the liquid thermal conductivity and the liquid transport factor. For the convenience of future reference, this product is named the liquid thermal conductance factor. Its values for several fluids are plotted in Fig. 3.4.

The foregoing are the relative operating characteristics of heat pipes in terms of the liquid transport factor, liquid thermal conductivity and liquid thermal conductance factor. The high values for the liquid-metal fluids, as can be seen in Figs. 3.2 through 3.4, indicate large heat transfer capability and small temperature drop for the high-temperature heat pipes. It is often possible to consider the high-temperature heat pipe as an isothermal device. On the other hand the low values for the cryogenic- and ambient-temperature fluids indicate that the temperature gradients is required to be considered for the low-temperature heat pipes.

2. Performance of High-Temperature Heat Pipes

As seen in the above section, the temperature gradient for high-temperature heat pipe is expected to be small. For

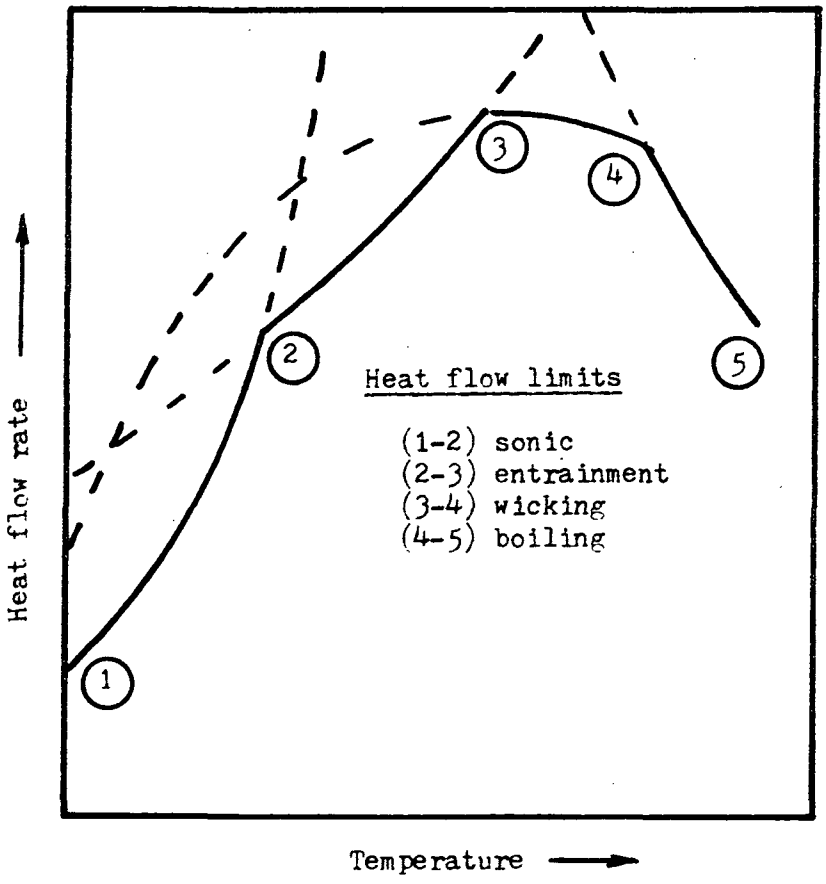

Figure 3.5 Heat pipe limitations[3]

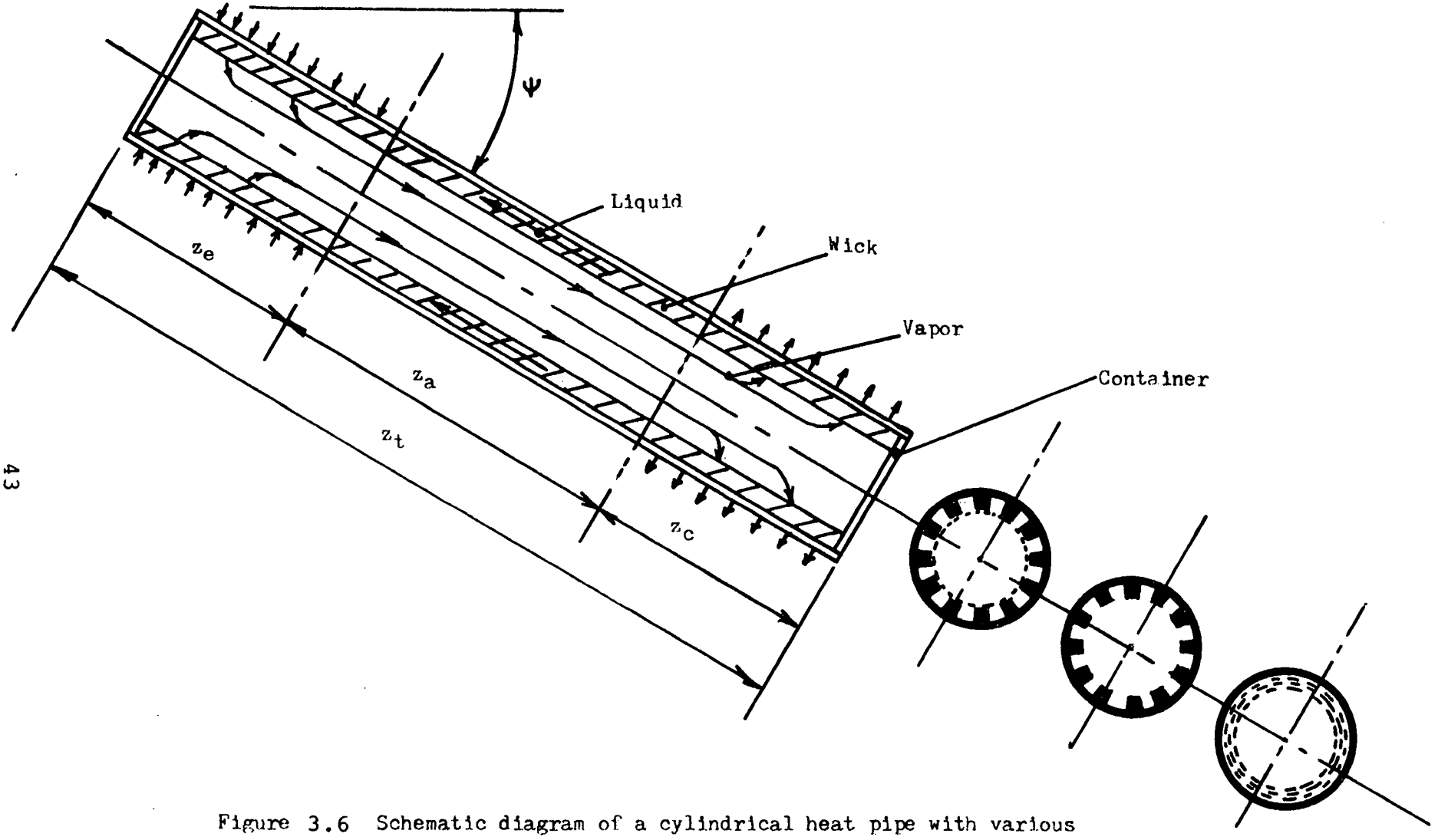

Figure 3.6 Schematic diagram of a cylindrical heat pipe with various wick structures

the performance, its heat-transfer capability is of main concern. Theories for the calculation of heat-transfer limitations have been developed by several authors, for example, see Refs. 2 and 3. Individual limitations indicated in Fig. 3.5 are considered by Kemme[3]. Following the work of Kemme, we derive a mathematical model for cylindrical high-temperature heat pipes at various wick structures as shown in Fig. 3.6.

Sonic limitation. The maximum Mach number at the evaporator exit is unity. For given values of vapor temperature and density at the upstream end of the evaporator T_g and ρ_g, the maximum mass flux density $\dot{m}''_{max}$ at the exit of the evaporator, assuming that vapor behaves like an ideal gas, can be calculated by Eq. 2.59, namely:

$$\dot{m}''_{max} = \rho_g \sqrt{\gamma R T_g / [2(\gamma+1)]}, \tag{2.59}$$

where the value of γ for monatonic gases in 1.667 and that for diatonic gases in 1.4. As the value of $\dot{m}''_{max}$ is related to the maximum heat transfer rate by the equation:

$$\dot{m}''_{max} = Q_{max}/(\pi r_g^2 h_{fg}). \tag{3.8}$$

Combination of Eqs. (2.59) and (3.9) results in an expression for sonic limitation:

$$Q_{max} = \rho_g h_{fg} \pi r_g^2 \sqrt{\gamma R T_g / [2(\gamma+1)]}. \tag{3.9}$$

Entrainment limitation. If the dynamic pressure of the vapor is excessive, some liquid from the wick-return system may be entrained. Once entrainment begins in a heat pipe, fluid circulation increases until the liquid-return path cannot accommodate the increased flow. This causes dryout and overheat of the evaporator. Weber number defined by Eq. (2.60) i.e., $Wb \equiv \rho_g \bar{u}^2 a/\sigma$, can be used as a criterion for the entrainment limitation. Magnitude of the characteristic length 'a' in the calculation of the Weber number is dependent upon the wick structures, which can be empirically determined for different structures once and for all. The entrainment limitation can then be determined by the equation

$$\rho_g \bar{u}^2 a/\sigma = 1. \tag{3.10}$$

As $\bar{u}$ is related to Q by the equation

$$\bar{u} = Q/(\pi r_g^2 \rho_g h_{fg}) \tag{3.11}$$

Substitution of Eq. (3.11) into (3.10) yields the following equation for entrainment limitation:

$$Q_{max} = \pi r_g^2 h_{fg} \sqrt{\sigma \rho_g / a} \ . \tag{3.12}$$

Wicking limitation. When the sum of pressure drops due to gravitational force and the resistance for liquid and vapor flows balances the maximum capillary pressure, wicking limitation is reached.

The maximum capillary pressure for a given liquid-wick combination can be calculated by Eq. (2.8), i.e.

$$\Delta p_c = 2\sigma \cos \theta / R_E \tag{3.13}$$

where θ is the liquid-wick wetting angle, and R_E is the effective capillary radius which equals to $2A/\wp$ for the meshed-screen wick and equals to $2A/(\wp-\omega)$ for the wick of open grooves.

The pressure drop due to gravitational force is calculated by Eq. (2.41), i.e.,

$$\Delta p_s = \rho_f g z_t \sin \psi. \tag{3.14}$$

The vapor pressure drop can be evaluated by integrating Eq. (2.9) with values of c_f for the evaporator and adiabatic section being calculated by Eq. (2.11). For the condenser at $|Re_w| < 4.5978$, c_f values can also be calculated by Eq. (2.11). However, $|Re_w|$ values at the condenser of heat pipes operating at this maximum heat-transfer capability are usually greater than 4.5978. Under this circumstance the reverse flow is likely to be developed at the condenser and the recovery of dynamic pressure at the condenser becomes difficult. At the present time, no quantitative information of pressure recovery at the condenser is available. It will be assumed that the dynamic pressure at the down-steam end of the adiabatic section will be lost at the condenser. The total pressure

can then be evaluated by integrating Eq. (2.9) from z = 0 to $z = z_e + z_a$ with c_f values for the evaporator and adiabatic section being calculated by Eq. (2.11), whence

$$\Delta p_g = \int_0^{z_e+z_a} 2\rho_g \bar{u}^2 / \{D_g Re[0.0481 + 0.0494/(4.7+Re_w)^{0.8}]\} + (8 \int_0^{D_g/2} \rho_g u^2 r dr / D_g^2)_{z=z_e+z_a} \quad (3.15)$$

The first integral of this Eq. (3.15) can be integrated in a straight-forward manner; and the second integral was investigated by Bohdansky et. al.[12] and Busse[13], whose results in the present notation may be written as:

$$(8 \int_0^{D_g/2} \rho_g u^2 r dr / D_g^2)_{z=z_d+z_a} = F(2\rho_g \bar{u}^2)_{z=z_e+z_a} \quad (3.16)$$

Where F in first approximation is equal to unit. For the case of uniform wall heat-flux density at the evaporator, Re_w for the evaporator may be written as $Q_{max}/\pi h_{fg} z_e \mu_g$, and $\bar{u}$ for the evaporator, and the adiabatic section can also be written in terms of Q_{max} as follows:

$$@\ Q \leq z \leq z_e: \quad \bar{u} = 4Q_{max} z/(\pi h_{fg} \rho_g D_g^2 z_e)$$

$$@\ a \leq z \leq (z_e+z_a): \quad \bar{u} = 4Q_{max}/(\pi h_{fg} \rho_g D_g^2) \quad (3.17)$$

Hence the following equation for Δp_g can be derived:

$$\Delta p_g = (Q_{max}/h_{fg})\{(4\mu_g/\pi\rho_g D_g^4)[z_e/(0.0481 + 0.0494/(4.7 + \frac{Q_{max}}{\pi h_{fg} z_e \mu_g})^{0.8}) + 32 z_a] + 32 Q_{max}/(\pi^2 \rho_g h_{fg} D_g^4)\} \quad (3.18)$$

The liquid pressure drop due to flow resistance can be evaluated by integration of Eq. (2.13), (2.22) or (2.23) depending on whether the capillary wick is made of wrapped screens, open grooves, or screen covered grooves. The resultant Δp_f expressions written in terms of Q_{max} are as follows:

For wrapped-screen screen wick:

$$\Delta p_f = cQ_{max}\mu_f(z_e+2z_a+z_c)/[2\pi\rho_f h_{fg}\varepsilon r_e^2(r_i^2-r_g^2)]. \tag{3.19a}$$

For open-groove wick:

$$\Delta p_f = 9Q_{max}\mu_f(\omega^2+4\delta^2)(z_e+2z_a+z_a)/(5n\rho_f h_{fg}\omega^3\delta^3). \tag{3.19b}$$

For screen-covered groove wicks:

$$\Delta p_f = 36\ Q_{max}\mu_f(\omega^2+\delta^2)(z_e+2z_a+z_c)/(5n\rho_f h_{fg}\omega^3\delta^3). \tag{3.19c}$$

In Eqs. (3.19b) and (3.19c), n is the number of grooves.

On the substitution of Eqs. (3.13), (3.14), (3.18) and (3.19) for the pressure differences Δp_c, Δp_s, Δp_g and Δp_f respectively into the following pressure-banance equation,

$$\Delta p_c = \Delta p_s + \Delta p_g + \Delta p_f, \tag{3.20}$$

the maximum heat-transfer rate due to wick limitation can be calculated.

Boiling limitation. Nucleate boiling in the wick structure of a heat pipe may interfere with the liquid return. The limiting temperature drop at the evaporator for the onset of nucleation can be calculated by Eq. (2.46), namely:

$$T_e - T_g = 2T_g\sigma/(h_{fg}\rho_g r_b), \tag{3.21}$$

where the value of the effective bubble radius is dependent upon the wick structure and it has to be determined empirically at the present time. $(T_e - T_g)$ may be written, in terms of the heat transfer rate, as follows:

$$(T_e - T_g) = Q_{max}(r_i - r_g)/[\pi K_e z_e (r_i + r_g)] \tag{3.22}$$

with the effective thermal conductivity, K_e, being evaluated by Eq. (2.26) for the wrapped-screen wicks and by Eq. (2.25) for the groove wicks. The value of porosity, ε, for the wrapped screen wick is dependent upon the wrapping tightness and the value of ε for the groove wick may be calculated by the equation

$$\varepsilon = n\omega/[\pi(r_i - r_g)] \tag{3.23}$$

Combination of Eqs. (2.26), (3.21) and (3.22) yields the following expression of boiling limitation for the wrapped-screen heat pipe:

$$Q_{max} = 2\pi T_g\sigma\{z_e(r_i+r_g)K_f[K_f+K_w-(1-\varepsilon)(K_f-K_w)]\}/\{(r_i-r_g)[K_f+K_w + (1-\varepsilon)(K_f-K_w)]h_{fg}\rho_g r_b\} \tag{3.24}$$

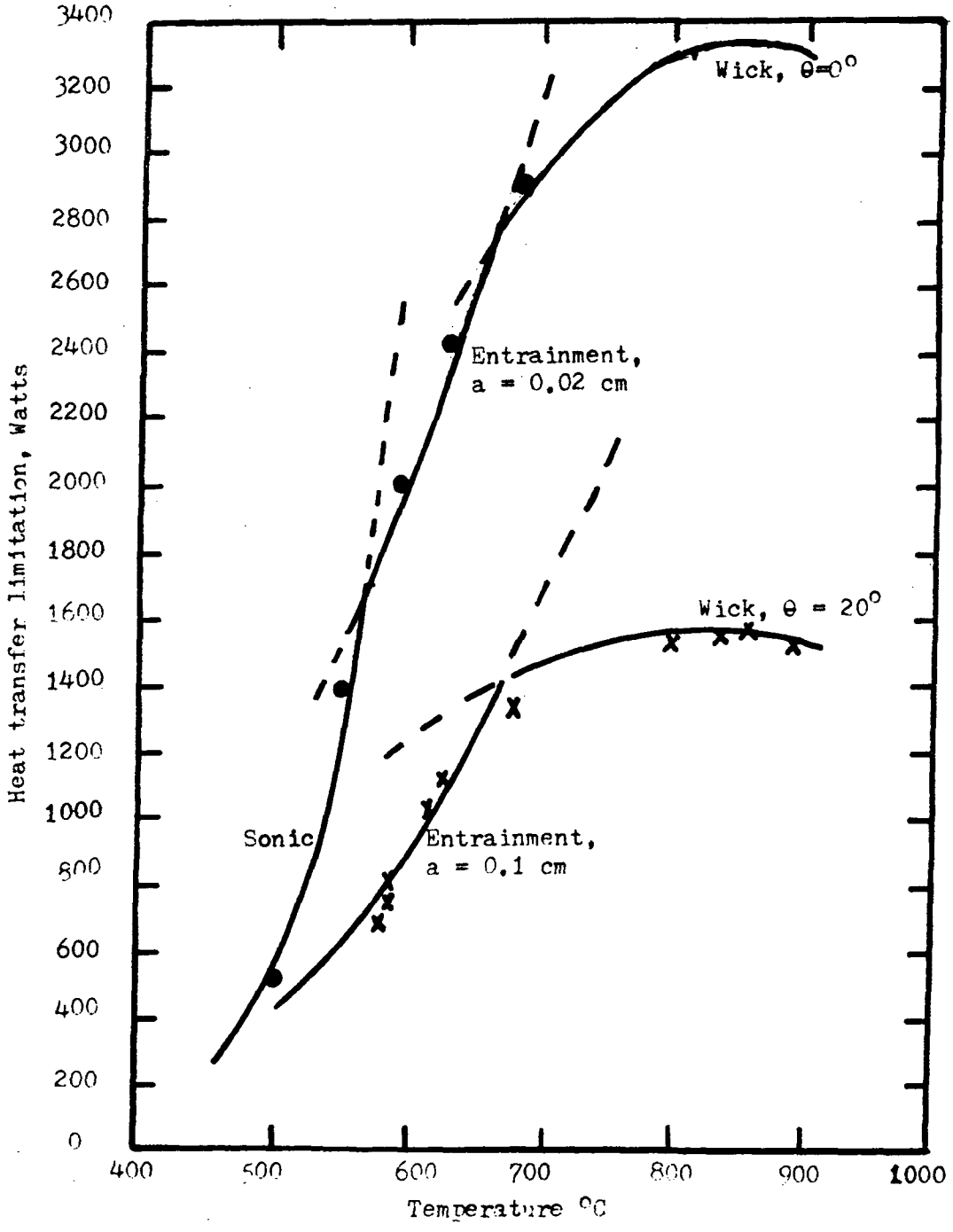

Fig. 3.7 Comparison of experimental and theoretical heat-pipe limitations. •, screen-covered groove wick; x, open-groove wick

and combination of Eqs. (2.25) and (3.21) through (3.23) gives the following expression of boiling limitation for the groove heat pipes:

$$Q_{max} = 2T_g\sigma z_e[n\omega K_f + [\pi(r_i+r_g)-n\omega]K_w\}/\{(r_i-r_g)h_{fg}\rho_g r_b\} \quad (3.25)$$

Computer program and comparison with experiments. A computer program has been written for the math model developed above for the calculation of heat transfer limitation. A program listing together with users instruction is appended to the manual, Appendix A.

An example of the calculated results using this program is shown in Fig. 3.7 for comparison with Kemme's experiments[15] under the same conditions. It can be seen in this figure that the experimental data are well represented by the theoretical prediction. However, it should be mentioned that values of the liquid-wick wetting angle θ, and the characteristic lengths 'a' for entrainment have been so chosen to give this good agreement.

3. Performance of Low-Temperature Heat Pipes

It was shown in Section I of this chapter that the temperature drops for the ambient- and low-temperature heat pipes are often important. Complete performance of these heat pipes will include not only the maximum heat transfer capability but also the temperature drops at various operating conditions. Accordingly a math model is developed to calculate these quantities.

Maximum heat-transfer capability. Because of the low values of liquid transport factor for the working fluids of the low temperature heat pipes, the most likely heat-transfer limitation is the wick limitation. Procedure for the calculation of wick limitation described in the above section for the high-temperature heat pipe is also applicable to the calculation of wick limitation for the low-temperature heat pipes. Thus the wick limitation is calculated by equating maximum capillary pressure Δp_c of Eq. (3.13) to the sum of the hydrostatic pressure drop Δp_s of Eq. (3.14), the vapor-flow pressure drop Δp_g of Eq. (3.18) and the liquid-flow pressure drop Δp_f of Eq. (3.19).

Temperature drop. The total temperature drop of a heat pipe is equal to the sum of temperature drops at the evaporator, vapor flow passage and condenser. Conduction model described in Section 5 of Chapter II can be used to calculate the temperature drops at the evaporator and condenser, respectively. The vapor pressure drop ΔT_g can be calculated by Clausius-Clopeyron Eq. (2.43)

$$\Delta T_g = T_g \Delta \bar{p}_g / (\rho_g h_{fg}), \tag{3.26}$$

where the average vapor pressure drop $\Delta \bar{p}_g$ is the difference of the average vapor pressures at the evaporator and the condenser; it can be calculated by Eq. (3.27a) or (3.27b) below

depending on whether $|Re_w|$ at condenser is less or greater than 4.5975:

$$\Delta\bar{p}_g = (2\mu_g Q/\pi h_{fg}\rho_g D_g^4)\{z_e/(0.0481 + 0.0494/(4.7+ \frac{Q}{\pi h_{fg} z_e \mu_g})^{0.8}) + 64z_a + z_c/(0.0481 + 0.0494/(4.7- \frac{Q}{\pi h_{fg} z_c \mu_g})^{0.8})\} \quad (3.27a)$$

or

$$\Delta\bar{p}_g = (Q/h_{fg})\{(2\mu_g/\pi\rho_g D_g^2)[z_e/(0.0481 + 0.0494/(4.7+ \frac{Q}{\pi h_{fg} z_e \mu_g})^{0.8}) + 64z_a] + 32Q/(\pi^2\rho_g h_{fg} D_g^4)\} \quad (3.27b)$$

These Eqs. (3.27a) and (3.27b) for $\Delta\bar{p}_g$ are obtained by integration of Eq. (2.9) using the procedure described in Section 2 of this chapter.

The temperature drop at the evaporator ΔT_e for thin wick structures can be calculated by the equation

$$\Delta T_e = Q(r_i - r_g)/[\pi z_e K_e (r_i + r_g)] \quad (3.28)$$

where K_e is the effective thermal conductivity of the liquid saturated wick which may be approximated by Eq. (2.26) for the wrapped screen wick and by Eq.(2.28) for the sintered-porous-metal wick. For wick structures composed of rectangular

grooves with $K_f << K_\omega$ evaporation occuring at the liquid-vapor interface but not at the groove fin tip, ΔT_e expression can be derived from Eq. (2.40), i.e.,

$$\Delta T_e = 0.185\ Q\ th\ [5.4(\delta/\omega)]/(nz_eK_f) \tag{3.29}$$

The temperature drop at the condenser ΔT_c for thin wick structures can be calculated by the equation

$$\Delta T_c = Q(r_i-r_g)/[\pi z_c K_e(r_i+r_g)] \tag{3.30}$$

where the effective thermal conductivity K_e for the liquid-saturated wrapped-screen and sintered-porous-metal wicks can again be calculated by Eqs. (2.30) and (2.28), respectively. For wicks of rectangular grooves condensation occurs at the liquid-vapor interface as well as the groove fin tips; and liquid and groove fin conduct heat in parallel. K_e can be calculated by Eq. (2.25), namely:

$$K_e = \varepsilon K_f + (1-\varepsilon)K_w \tag{3.31}$$

where ε is equal $n\omega/[\pi(r_i+r_g)]$.

Computer program and comparison with experiments. A computer program for the above described math model for the low temperature heat pipe has been developed; both maximum heat transfer capability and total temperature drops are calculated at various operating conditions. The program is applicable to the heat pipe with wrapped-screen wick, open-rectangular-groove wick or screen-covered-rectangular-groove wick. The

program listing together with users instruction is given in Appendix B.

The calculated evaporator temperature drop for a liquid nitrogen heat pipe with wrapped-screen wick is plotted versus heat transfer rate in Fig. 3.8 for comparison with Haskin's experimental data under the same operating conditions. Predictions based upon the present conduction model closely represents the empirical data. Also shown in Fig. 3.8 are the evaporator temperature drops calculated by the theories of nucleate pool boiling Eq. (2.48), and nucleate boiling in wick structures Eq. (2.49). It can be seen in this Fig. 3.8 that nucleate boiling heat transfer theory underestimate the evaporate temperature drop. For further improvement on the present conduction model, liquid property variation with respect to temperature and convection heat transfer should be accounted, as can be seen in Figs. 3.9 and 3.10. Details of conduction evaporation model with convection and property variation considered are described in Ref. 14.

The low temperature heat pipes with the wrapped screen wicks have rather poor performance from the temperature-drop point of view as can be seen in Fig. 3.10. The grooved heat pipe offers improvement in both the heat transfer capability and the effective thermal conductance, because the grooves provide a small liquid flow resistance for liquid return and

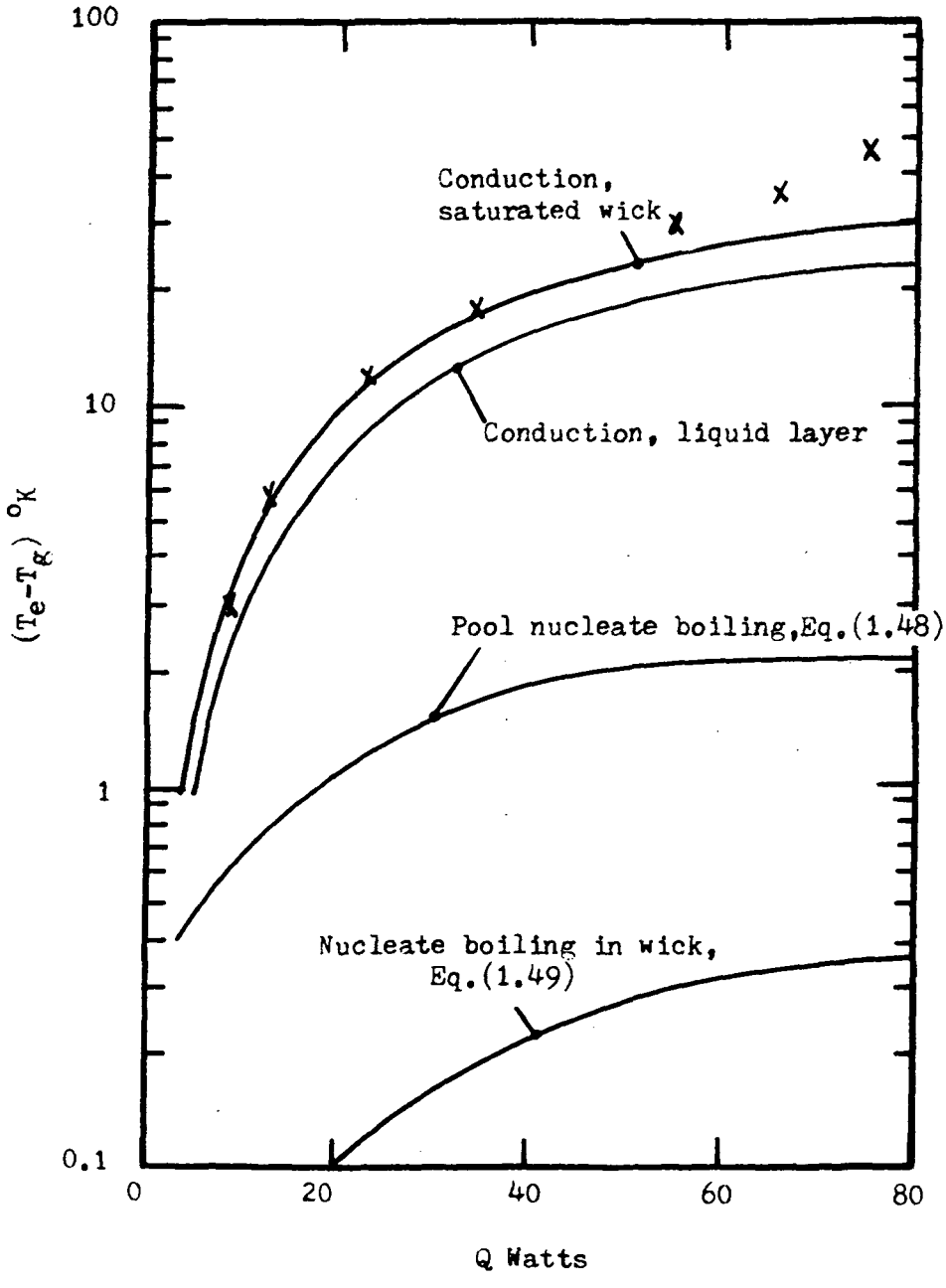

Figure 3.8 Comparison of evaporation heat transfer theories with experiments

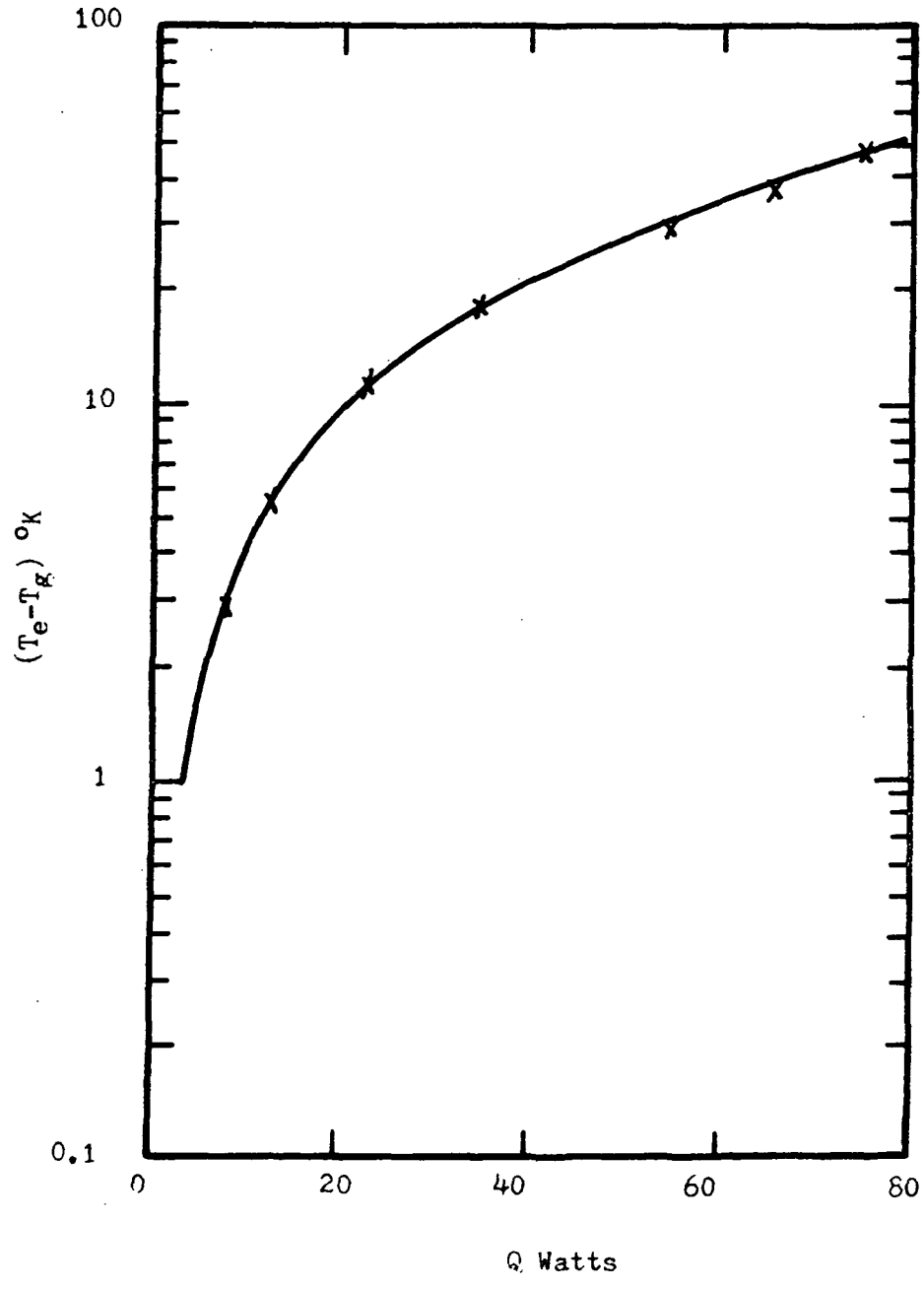

Figure 3.9 Evaporation based upon conduction model taking into account of convection and fluid property variations

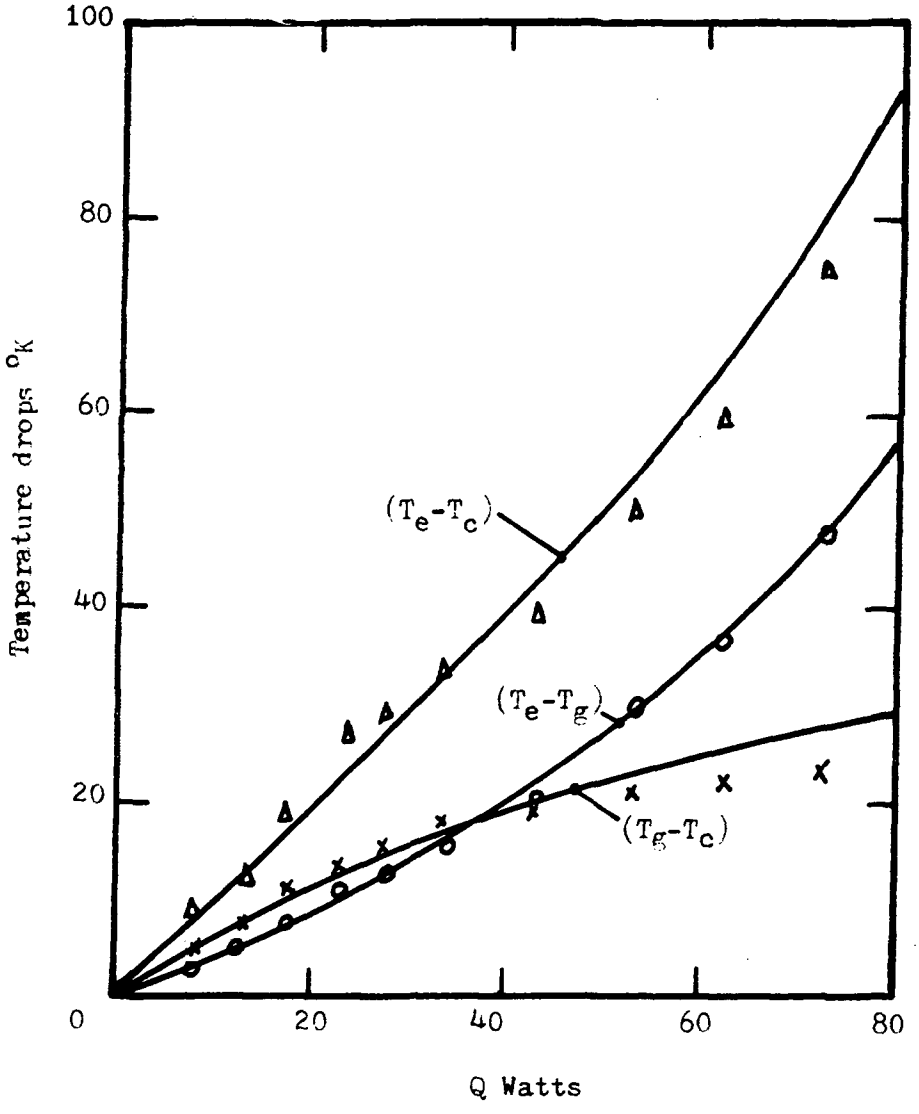

Figure 3.10 Condenser, evaporator and total temperature drops of a LN_2 heat pipe -- A comparison between theory and experiments

the highly conductive groove fins insure low resistance for heat flow.

The present predictions for the heat transfer capability and temperature drops of a Dynatherm liquid nitrogen heat pipe with groove wicks are shown in Figs. 3.11 and 3.12 for comparison with the experiments[16] by Dynatherm under the same conditions.

The above Dynatherm nitrogen cryopipe is used as an example to illustrate the use of the present computer program to generate complete performance of the low-temperature heat pipes. This heat pipe has the following specifications:

Mean groove height, δ	0.089	cm
Mean groove width, ω	0.064	cm
Inner diameter, D_i	0.97	cm
Outer diameter, D_o	1.27	cm
No. of grooves, n	30	
Evaporator length, z_e	10	cm
Adiabatic-section length, z_a	120	cm
Condenser length, z_c	10	cm
Empirical capillary radius, R_E	0.0354	cm
Container material	6061-76Al	

The predicted complete performance of this heat pipe is shown in Fig. 3.13 in which the locus of the maximum heat-transfer capability and the lines of constant rate of heat transfer are mapped on the total temperature-drop versus condenser-temperature coordinates.

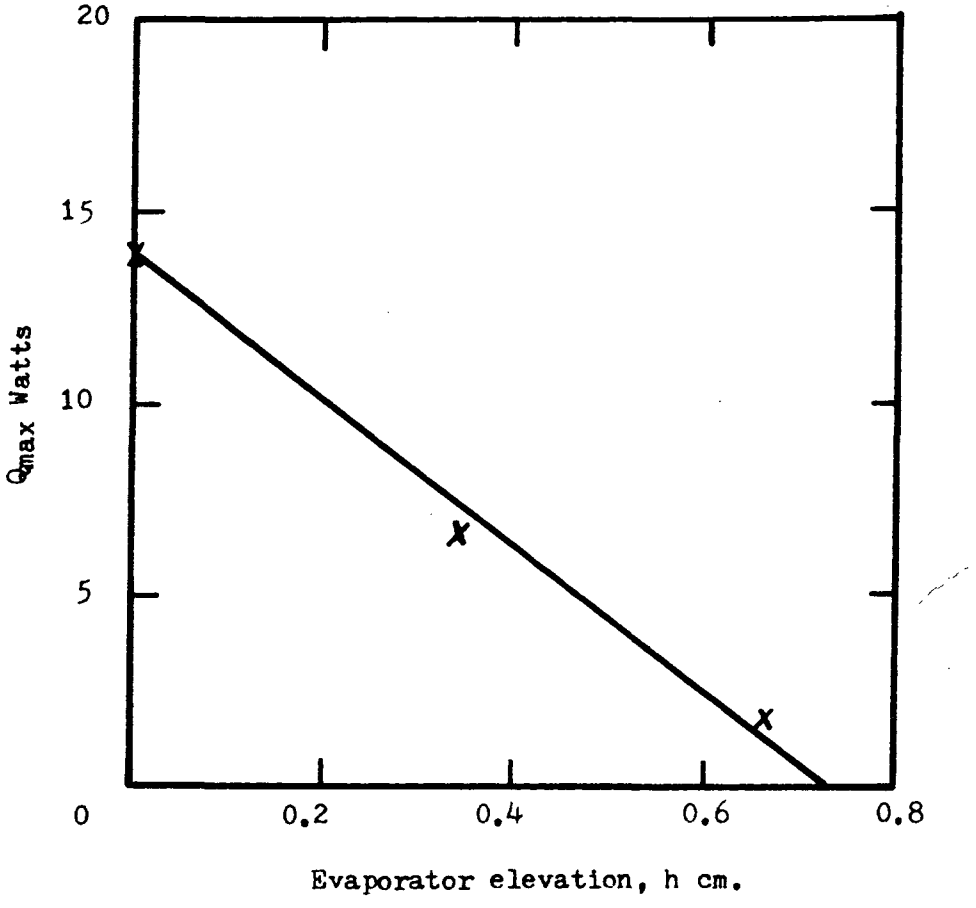

Figure 3.11 Comparison of theoretical heat transfer limitation of a grooved LN_2 heat pipe with experimental data

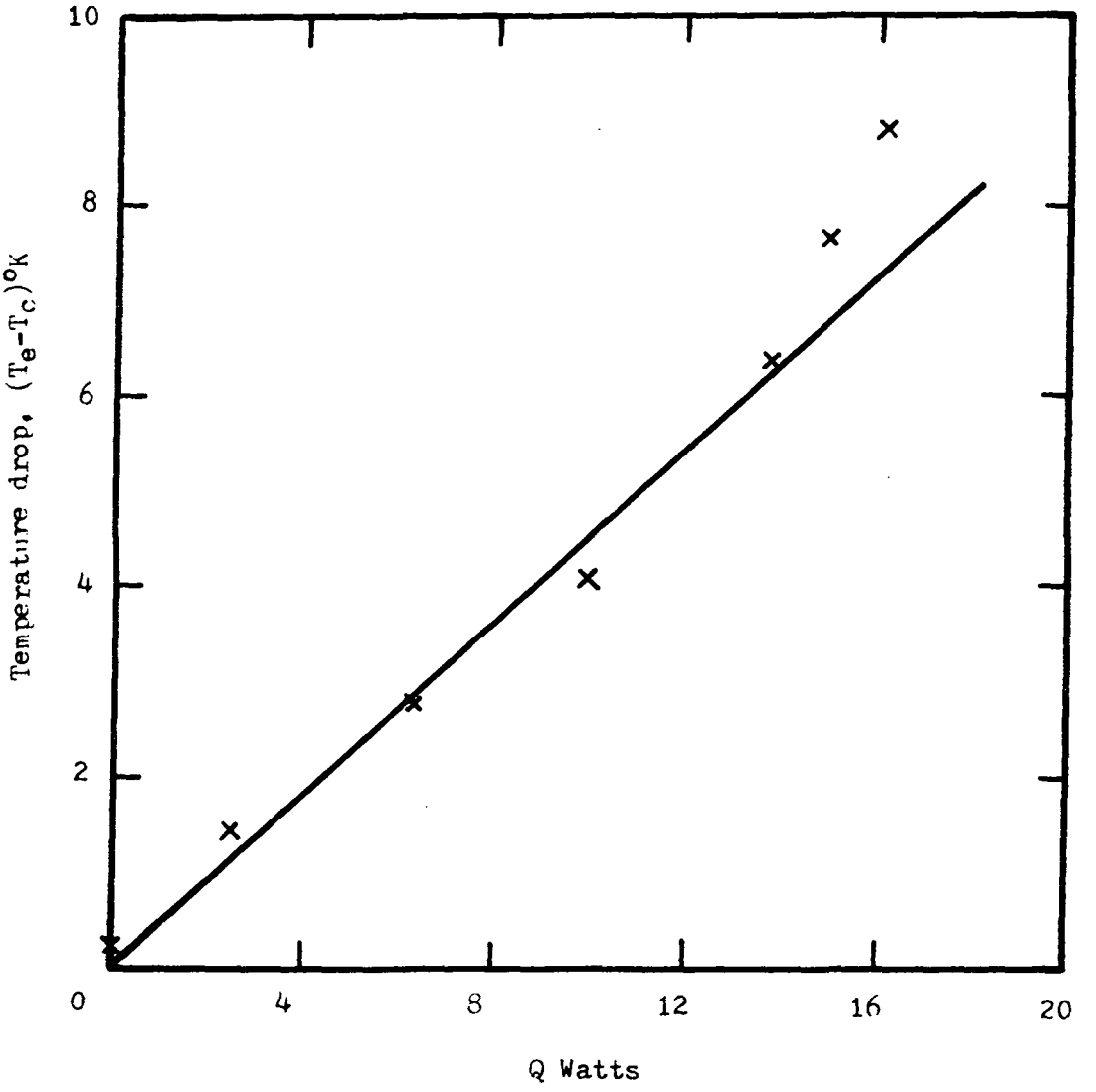

Figure 3.12 Comparison of theoretical temperature drop of a grooved LN_2 heat pipe with experiments

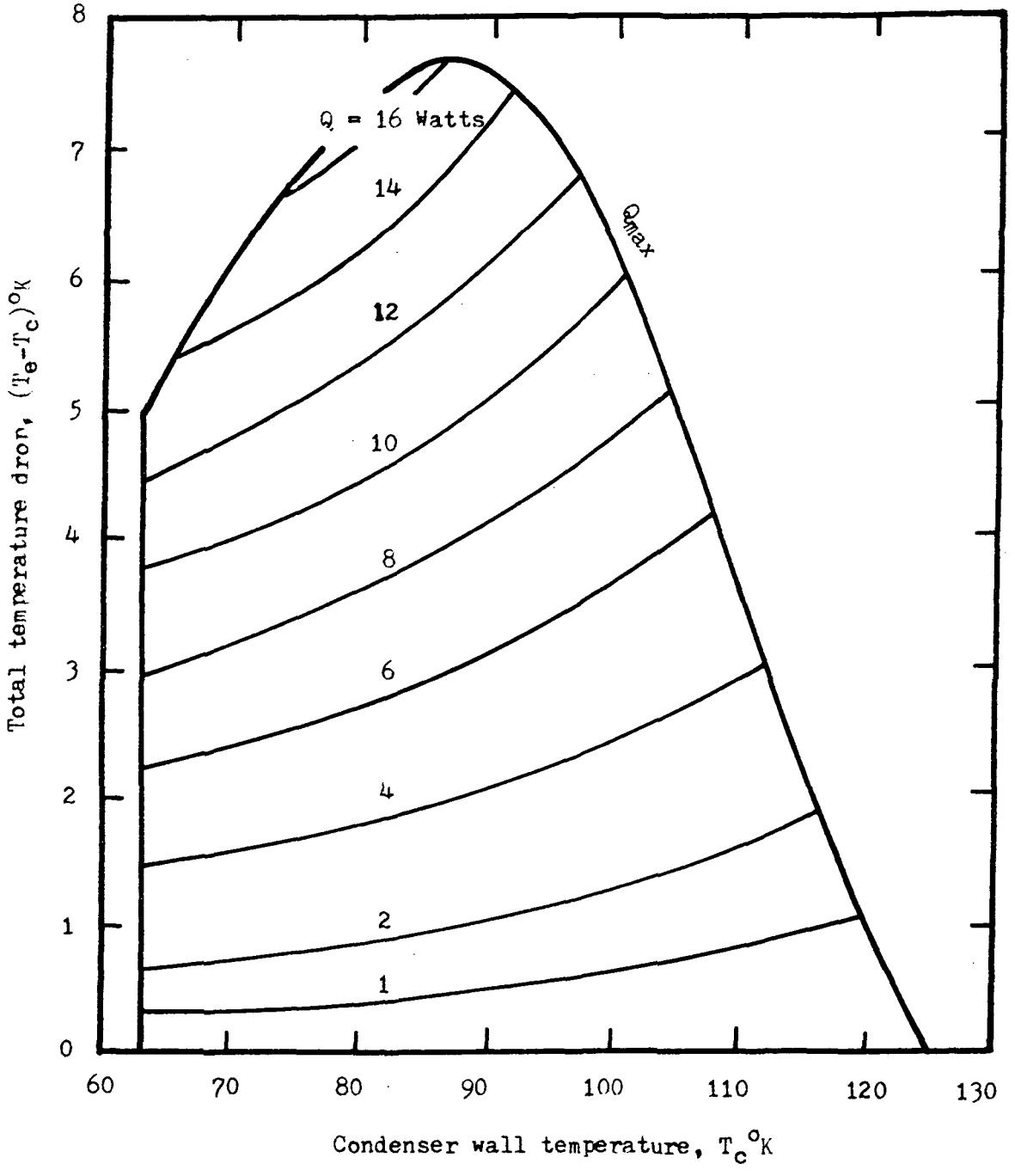

Figure 3.13 Predicted performance of a grooved LN_2 heat pipe

IV. CONCLUSIONS AND RECOMMENDATIONS

1. Conclusions

In conclusion the results of this research can be summarized as follows:

(i) Fundamentals of heat and mass transfer theory are reviewed with a view of application to theoretical analyses of heat pipes of various wick structures and working fluids.

(ii) A math model for high-temperature heat pipes has been developed by means of which it is possible to predict the heat-transfer limitations of heat pipes with wrapped-screen, rectangular-groove or screen-covered-rectangular-groove wick.

(iii) A math model for low temperature heat pipes with wrapped-screen, rectangular-groove or screen-covered-rectangular-groove wick has also been developed by means of which complete performance of heat pipes (e.g., see Fig. 3.3) including both heat transfer limitations and temperature gradients at different operating conditions can be predicted.

(iv) The extent to which the present prediction correlates the existing experimental data can be judged by inspection of Figs. 3.7, 3.11 and 3.12.

(v) The theory is capable of greater refinement when more comprehensive experimental data become available.

2. Recommendations

It is recommended that the present theory should be extended and developed in the following ways:

(i) There is a need for comprehensive experimental data in particular those for the low temperature heat pipes. Initial work confined to a single low-temperature heat pipe at different operating conditions would be fruitful, particularly with the aim of obtaining complete performance of a heat pipe as shown in Fig. 3.13. The next step would carry out tests on the same heat pipe with a variety of working fluids and combinations of evaporator, adiabatic-section and condenser lengths.

(ii) Laminar and turbulent tube flows with mass injection have been reasonably well understood. By comparison, knowledge of laminar and turbulent tube flows with large wall suction is limited at the present time. Both theoretical and experimental data on tube flows with large suction are urgently needed to increase confidence in calculating pressure drops due to vapor flow resistance.

(iii) Mechanisms of heat and mass transfer in groove wick are not well understood at the present time. Detailed studies should now be made.

(iv) When the data recommended above become available, complete performance of heat pipe will be able to be developed with greater assurance of its accuracy.

V. REFERENCES

1. Shelpuk, B., Crouthamel, M. S., and Cygnarowicz, T. A., "ICICLE: Integrated cryogenic isotope cooling engine system," ASME Paper No. 70-HT/SpT-30, (1970).
2. Cotter, T.P., "Theory of Heat Pipes," Los Alamos Scientific Laboratory, Rept. No. LA-3246-MS, (1965).
3. Kemme, J.E., "Heat pipe design considerations," Los Alamos Scientific Laboratory, Rept. No. LA-4221-MS, (1969).
4. Bressler, R.G., and Wyatt, P.W., "Surface wetting through capillary grooves," AIChE-ASME 11th National Heat Transfer Conference, AIChE Preprint 19, (1963).
5. Yuan, S.W., and Finkelstein, A.B., "Laminar flow with injection and suction through a porous wall," Heat Transfer and Fluid Mechanics Institute, Los Angeles, (1955).
6. Raithby, G., "Laminar heat transfer in the thermal entrance region of circular tubes and two-dimensional rectangular ducts with wall suction and injection," Int. J. Heat Mass Transfer, Vol. 14, pp. 223-243, (1971).
7. Schlichting, H., "Boundary-Layer Theory," 6th ed., McGraw-Hill, New York, N.Y., (1968).
8. Kantorovich, L.V., and Koylov, V.I., "Approximate Methods of Higher Analysis," Interscience, New York, N.Y., (1964).
9. Gorring, R.L., and Churchill, S.W., "Thermal conductivity of Heterogeneous materials," Chemical Engineering Progress, Vol. 57, No. 7, pp. 53-59, (1961).

10. Rohsenow, W.M., "A method of correlating heat transfer data for surface boiling of liquids," Trans. ASME, Vol. 48, (1952); Also see Rohsenow, W.M., and Choi, H.Y., "Heat, Mass and Momentum Transfer," Prentice-Hall, Englewood Cliffs, N.J., (1961).

11. Allingham, W.D., and McEntire, T.A., "Determination of boiling film coefficient for a heated horizontal tube in water-saturated wick material," J. Heat Transfer, Vol. 83, pp. 71-76, (1961).

12. Bohdansky, J., Strub, H., and van Andel, E., "Heat transfer measurements using a sodium heat pipe working at low vapor pressure," Proc. Thermionic Conversion Specialist Conference, Houston, Texas, Nov. 3-4, (1966).

13. Busse, C.A., "Pressure drop in the vapor phase of long heat pipes," Proc. Thermionic Conversion Specialist Conference, Palo Alto, California, Oct. 30-Nov. 1, (1967).

14. Chi, S.W., and Cygnarowicz, T.A., "Theoretical analyses of cryogenic heat pipes," ASME Paper No. 70-HT/SpT-6, (1970).

15. Kemme, J.E., "Heat pipe capability experiments," Los Alamos Scientific Laboratory, Rept. No. LA-3585-MS, (1966).

16. Annon, "Cryogenic grooved heat pipes," A report submitted by Dynatherm Corp. to NASA-Goddard Space Flight Center, (1971).

17. Bienert, W.B., "Heat pipes for temperature control," Proc. of the 4th Intersociety Energy Conversion Engineering Conference, pp. 1033-1041, (1969).

18. Marcus, B.D., and Fleischman, G.L., "Steady-state and transient performance of hot reservoir gas controlled heat pipes," ASME Paper No. 70-HT/SpT-11, (1971).

APPENDIX A

A COMPUTER PROGRAM FOR LIMITATIONS OF HIGH TEMPERATURE HEAT PIPES

A complete listing of the computer program in Fortran IV language for calculation of sonic, entrainment, wick and boiling limitations is given in this Appendix. This program is written for application to the wrapped-screen-wick, open rectangular-groove and screen-covered rectangular-groove heat pipes. Also given in this Appendix are the flow diagram of the program (Fig. A1), and the data input sheets (Table A1). All the integers, beginning with I through N, at the input are 5-digit figures (I5); and all other inputs are 15-digit figures (E15.6). The main Fortran input and output symbols are defined as follows:

Input:

GRF	gravitational constant, 981 cm/sec^2
ND	number of sets of heat-pipe physical dimensions
NTHP	type of heat pipes; i.e., 1 for wrapped screen, 2 for open groove, and 3 for screen covered groove
RG	radius of vapor flow passage, cm
RI	inner radius of heat-pipe container, cm
ZE	length of evaporator, cm
ZA	length of adiabatic section, cm
ZC	length of condenser, cm
PSI	inclination of heat pipe, radian
RB	effective bubble radius for boiling, cm
THETA	liquid wetting angle, radian
A	characteristic length for entrainment, cm

CDWK	thermal conductivity of wick material, erg/cm sec °K
RF	effective hydraulic radius for liquid flow, cm
C	permeability factor for capillary structure, a non-dimensional constant
EPSIL	porosity of capillery structure
AREA	cross-sectional area of capillary pores or capillary grooves, cm
PERI	wetted perimeter of capillary pores or capillary grooves, cm
GRVN	number of capillary grooves
WIDTH	width of capillary grooves
DEPTH	depth of capillary grooves
NP	number of sets of fluid property input
TSAT	fluid saturation temperature, °K
PSAT	saturation vapor pressure, dyne/cm^2
CPF	saturation liquid specific heat, ergs/gm °K
DENF	saturation liquid density, gm/cm^3
VSF	saturation liquid viscosity, poise
CDF	saturation liquid thermal conductivity
SFT	saturation liquid surface tension, dyne/cm
HFG	heat of vaporization, erg/gm
DENG	saturation vapor density, gm/cm
VSG	saturation vapor viscosity, poise
GAMMA	vapor specific heats ratio

Output

ZE	length of evaporator, cm
ZA	length of adiabatic section, cm
ZA	length of condenser, cm
PSI	heat-pipe inclination, radian
A	characteristic length for entrainment, cm
THETA	liquid wetting angle, radian
RB	effective bubble radius for boiling, cm
TSAT	heat-pipe vapor temperature, °K

QS	sonic limitation, erg/sec
QEL	entrainment limitation, erg/sec
QWL	wick limitation, erg/sec
QBL	boiling limitation, erg/sec
QMAX	ultimate heat-pipe limitation (i.e., smallest of QSL, QEL, QWL, QBL), erg/sec.

(NOTE: 1 watt = 10^7 ergs/sec)

Fig. A1 Flow diagram of program for performance of high-temperature heat pipe

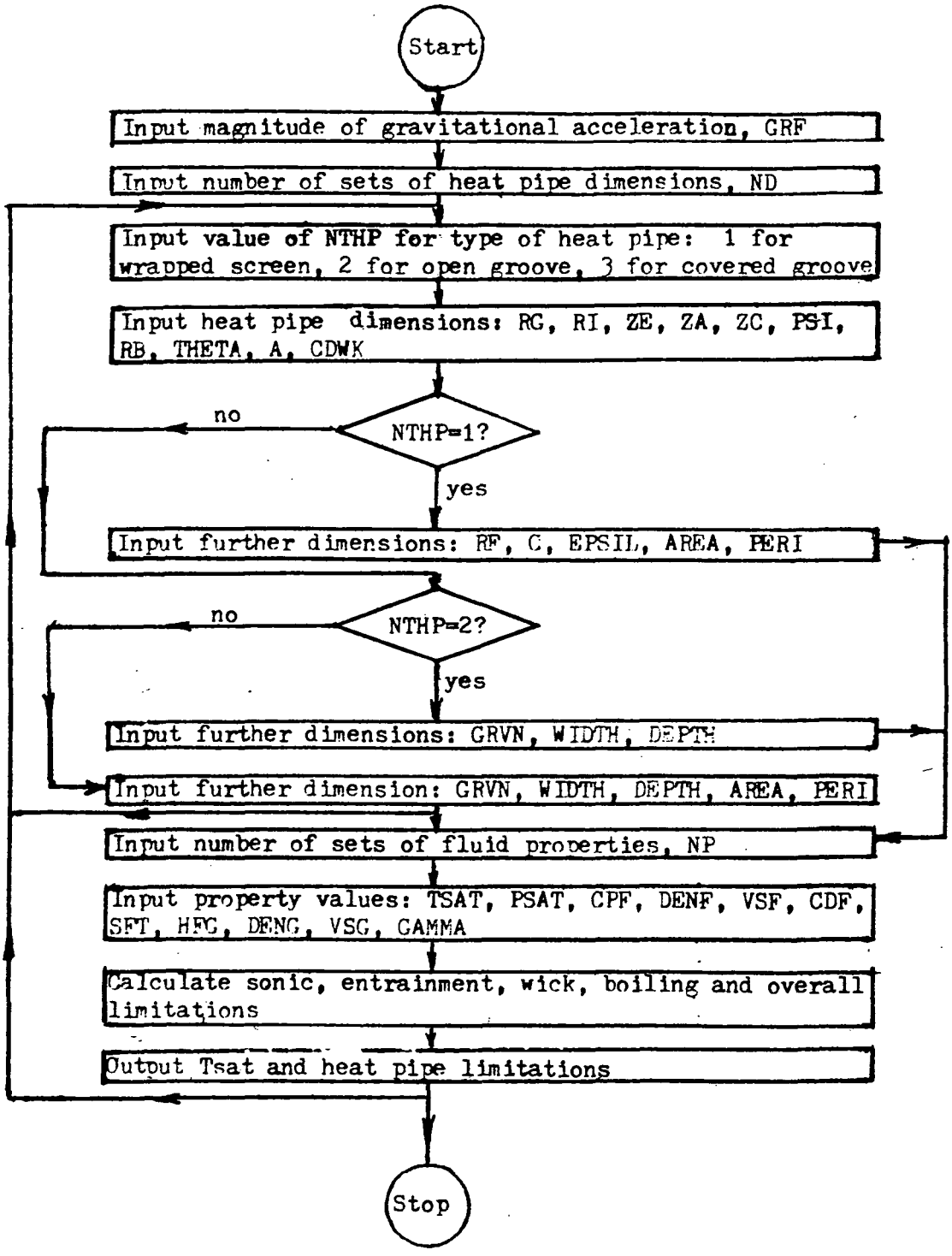

TABLE A1 (a)

INPUT DATA FOR WRAPPED-SCREEN HEAT PIPE

GRF			
ND			
NTHP (=1)			
RG	RI		
ZE	ZA	ZC	PSI
RB	THETA	A	CDWK
RF	C	EPSIL	
AREA			
NP			
TSAT	PSAT	CPF	
DENF	VSF	CDF	SFT
HFG	DEVG	VSG	
GAMMA			

TABLE A1 (b)

INPUT DATA FOR OPEN-GROOVE HEAT PIPES

GRF			
ND			
NTHP (=2)			
RG	RI		
ZE	ZA	ZC	PSI
RB	THETA	A[	CDWK
GRVN	WIDTH	DEPTH	
NP			
TSAT	PSAT	CPF	SFT
DENF	VSF	CDF	SFT
HFG	DENG	VSG	
GAMMA			

TABLE A1 (c)

INPUT DATA FOR SCREENED-COVERED-GROOVE HEAT PIPES

GRF				
ND				
NTHP	(= 3)			
RG		RI		
ZE		ZA	ZC	PSI
RB		THETA	A	CDWK
GRVN		WIDTH	DEPTH	
AREA		PERI		
NP				
TSAT		PSAT	CPF	
DENF		VSF	CDF	SFT
HFG		DENG	VSG	
GAMMA				

```
      $JOB (7352,F),'CHI,J'
      C PERFORMANCE OF HIGH-TEMPERATURE HEAT PIPES
    1    20 FORMAT (//43H PERFORMANCE OF HIGH-TEMPERATURE HEAT PIPES)
    2       WRITE (6,20)
    3     1 FORMAT (I5)
    4    21 FORMAT (///56H       ZE                ZA                ZC
         1 PSI)
    5    22 FORMAT (/37H       A                 THETA             RB)
    6    11 FORMAT (E15.6)
    7    12 FORMAT (2E15.6)
    8    13 FORMAT (3E15.6)
    9    14 FORMAT (4E15.6)
   10    16 FORMAT (6E15.6)
   11       READ (5,11)GRF
   12       READ (5,1) ND
   13       DO 101 MD=1,ND
   14       READ (5,1) NTHP
   15       READ (5,12) RG,RI
   16       DG=2.*RG
   17       READ (5,14) ZE,ZA,ZC,PSI
   18       READ (5,14) RB,THETA,A,CDWK
   19       IF (NTHP - 1) 35,31,35
   20    35 IF (NTHP-2) 33,32,33
   21    31 READ (5,13) RE,C,EPSIL
   22       READ  (5,12) AREA,PERI
   23       RE=2.*AREA/PERI
   24       GO TO 34
   25    32 READ (5,13) GRVN, WIDTH,DEPTH
   26       RE=WIDTH
   27       GO TO 34
   28    33 READ (5,13) GRVN, WIDTH, DEPTH
   29       READ (5,12) AREA,PERI
   30       PE = 2.*AREA/PERI
   31    34 READ (5,1) NP
   32       WRITE (6,21)
   33       WRITE (6,14) ZE,ZA,ZC,PSI
   34       WRITE (6,22)
   35       WRITE (6,13) A,THETA,RB
   36       WRITE (6,23)
   37       DO 102 MP=1,NP
   38       READ (5,13) TSAT,PSAT,CPF
   39       READ (5,14) DENF,VSF,CDF,SFT
   40       READ (5,13) HFG,DENG,VSG
   41       READ (5,11) GAMMA
   42       QSL=DENG*HFG*3.14159*RG*RG*SQRT(GAMMA*PSAT/(2.*DENG*(GAMMA+1.)))
   43       QEL=3.14159*RG*PG*HFG*SQRT(SFT*DENG/A)
   44       DPC=2.*SFT*COS(THETA)/RE
   45       DPS=DENF*GRF*(ZE+ZA+ZC)*SIN(PSI)
   46       IF (NTHP-1) 45,41,45
   47    45 IF (NTHP -2) 43,42,43
   48    41 DPF=C*VSF*(ZE+2.*ZA+ZC)/(2.*3.14159*DENF*HFG*EPSIL*RE*RE)
   49       DPF=DPF/(RI*RI-RG*RG)
   50       QBL=3.14159*TSAT*SFT*ZE* CDF*(RI+RG)
   51       QBL=QBL*(CDF+CDWK-(1.-EPSIL)*(CDF-CDWK))
   52       QBL=QBL/(HFG*DENG*RB*(RI-RG))
   53       QBL=QBL/(CDF+CDWK+(1.-EPSIL)*(CDF-CDWK))
   54       QBL=2.*QBL
   55       GO TO 44
   56    42 DPF=9.*VSF*(WIDTH**2+4.*DEPTH**2)*(ZE+2.*ZA+ZC)
   57       DPF=DPF/(5.*GRVN*DENF*HFG*(WIDTH**3)*(DEPTH**3))
```

```
58          QBL=2.*TSAT*SFT*(GRVN*WIDTH*CDF+(3.14159*(RI+RG)-GRVN*WIDTH)*CDWK)
           1 *ZE/((RI-RG)*HFG*DENG*RB)
59          GO TO 44
60       43 DPF=36.0*VSF*(WIDTH**2+DEPTH**2)*(ZE+2.*ZA+ZC)
61          DPF=DPF/(5.*GRVN*DENF*HFG*(WIDTH**3)*(DEPTH**3))
62          QBL=2.*TSAT*SFT*(GRVN*WIDTH*CDF+(3.14159*(RI+RG)-GRVN*WIDTH)*CDWK)
           1/((RI-RG)*HFG*DENG*RB)
63       44 DPG2=32./(3.14159*3.14159* DENG*HFG*HFG*DG**4)
64          DPGX=4.*VSG/(3.14159*DENG*HFG*DG**4)
65          DO 103 M=1,5
66          IF (M-1) 52,51,52
67       51 DPG1=DPGX*(21.*ZE+32.*ZA)
68          GO TO 53
69       52 DNM=EXP(0.8*ALOG(4.7+QWL/(3.14159*HFG*ZE*VSG)))
70          DNM=0.0481+0.0494/DNM
71          DPG1=DPGX*(ZE/DNM+32.*ZA)
72       53 IF (DPS-DPC) 61,60,60
73       60 QWL=0
74          GO TO 103
75       61 AQ=DPG2
76          BQ=(DPF+DPG1)/2.
77          CQ=DPS-DPC
78      103 QWL=(-BQ+SQRT(BQ*BQ-AQ*CQ))/AQ
79       23 FORMAT (//87H        TSAT                QS                QEL
           1 QWL              QBL              QMAX)
80          IF (QSL-QEL) 71,71,72
81       71 QMAX=QSL
82          GO TO 73
83       72 QMAX=QEL
84       73 IF (QMAX-QWL) 74,74,75
85       75 QMAX=QWL
86       74 IF (QMAX-QBL) 76,76,77
87       77 QMAX=QBL
88       76 WRITE (6,16) TSAT,QSL,QEL,QWL,QBL,QMAX
89      102 CONTINUE
90      101 CONTINUE
91          CALL EXIT
92          STOP
93          END
```

APPENDIX B

A COMPUTER PROGRAM FOR PERFORMANCE OF LOW-TEMPERATURE HEAT PIPES

A complete listing of the computer program in Fortran IV language for calculation of complete performance of cryogenic and ambient-temperature heat pipes is given in this Appendix; both the maximum heat transfer capability and the evaporator- as well as the condenser-wall temperatures at various heat transfer rates are predicted. This program is applicable to the wrapped-screen-wick, open rectangular-groove and screen-covered rectangular-groove heat pipes. Also given in this Appendix are the flow diagram of the program (Fig. B1) and the data input sheets (Table B1). All the integers, beginning with I through N, at the input are 5-digit figures (I5); and all other inputs are 15-digit figures (E15.6). The main FORTRAN input and output symbols are defined as follows:

Input

NQ	number of heat transfer rates at which the evaporator and condenser temperatures are calculated, ergs/sec.
QI	initial heat transfer rates for temperature calculations, ergs/sec
DQ	stepwise increase of heat transfer rates for temperature calculations, ergs/sec.

(All other input symbols are same as those defined in APPENDIX A)

Output

ZE	length of evaporator, cm
ZA	length of adiabatic section, cm
ZC	length of condenser, cm
PSI	angle of inclination of heat pipe, radian
THETA	liquid wetting angle, radian
TSAT	saturation vapor temperature, °K
QMAX	maximum heat transfer capability, ergs/sec
TE	evaporator wall temperature, °K
TC	condenser wall temperature, °K
DT	temperature difference between the evaporator and the condenser walls, °K

Fig. B1 Flow diagram of program for performance of low-temperature heat pipe

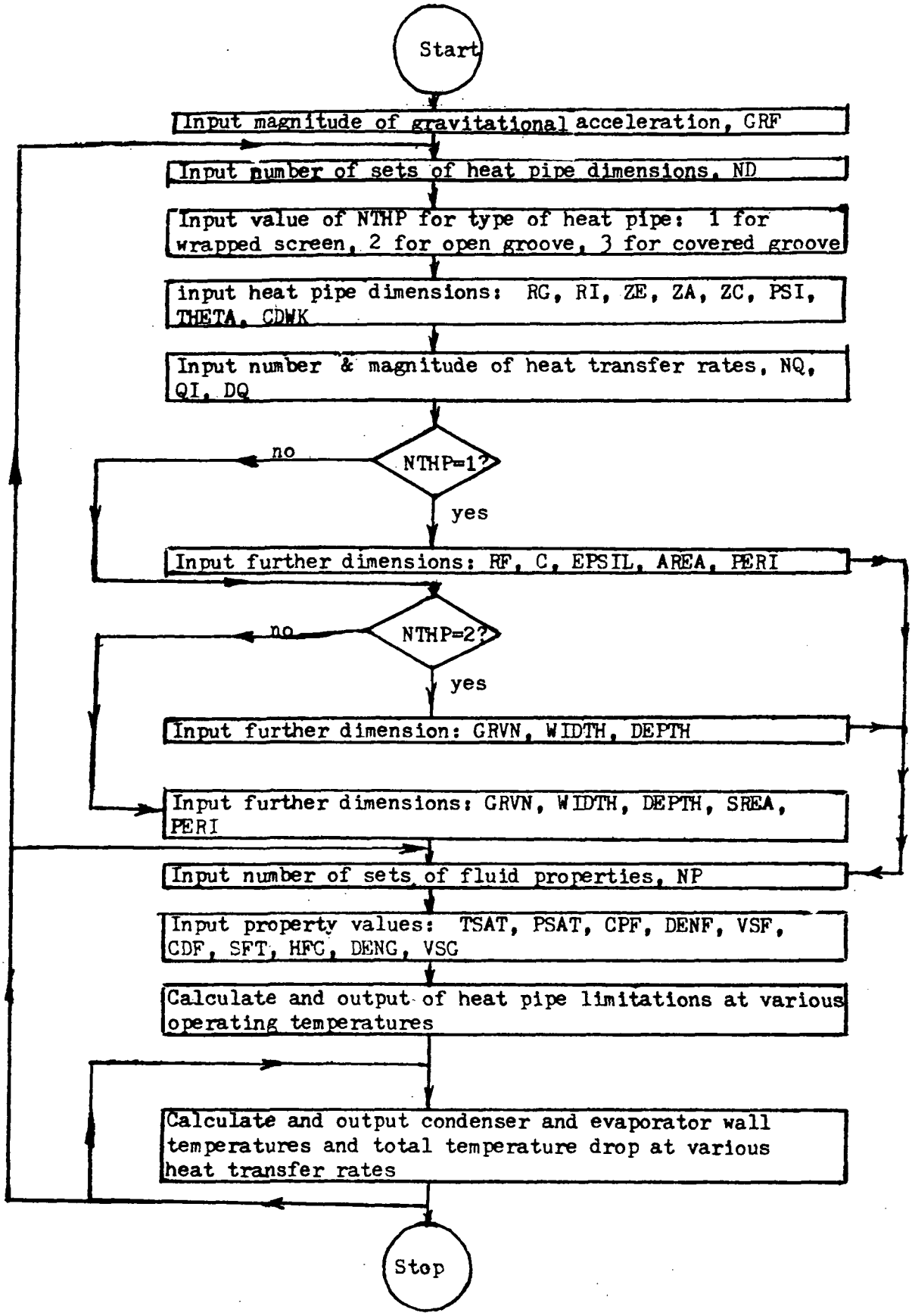

TABLE B1 (a)

INPUT DATA FOR WRAPPED-SCREEN HEAT PIPE

GRF			
ND			
NTHP (= 1)			
RG	RI		
ZE	ZA	ZC	PSI
THETA	CDWK		
NQ			
QI	DQ		
RF	C	EPSIL	
AREA	PERI		
NP			
TSAT	PSAT	CPF	
DENF	VSF	CDF	SFT
HFG	DENG	VSG	

TABLE B1 (b)

INPUT DATA FOR OPEN-GROOVE HEAT PIPE

GRF			
ND			
NTHP (= 2)			
RG	RI		
ZE	ZA	ZC	PSI
THETA	CDWK		
NQ			
QI	DQ		
GRVN	SIDTH	DEPTH	
NP			
TSAT	PSAT	CPF	
DENF	VSF	CDF	SFT
HFG	*DENG*	*VSG*	

TABLE B1 (c)

INPUT DATA FOR SCREEN-COVERED-GROOVE HEAT PIPES

GRF			
ND			
NTHP (= 3)			
RG	RI		
ZE	ZA	ZC	PSI
THETA	CDWK		
NQ			
QI	DQ		
GRVN	WIDTH	DEPTH	
AREA	PERI		
NP			
TSAT	PSAT	CPF	
DENF	VSF	CDF	SFT
HFG	DENG	VSG	

```
      $JOB (7352,F),'CHI,J'
      C PERFORMANCE OF LOW TEMPERATURE HEAT PIPES
    1    20 FORMAT (///42H PERFORMANCE OF LOW-TEMPERATURE HEAT PIPES)
    2       WRITE (6,20)
    3     1 FORMAT (I5)
    4    11 FORMAT (E15.6)
    5    12 FORMAT (2E15.6)
    6    13 FORMAT (3E15.6)
    7    14 FORMAT (4E15.6)
    8    15 FORMAT (5E15.6)
    9       READ (5,11) GRF
   10       READ (5,1) ND
   11       DO 101 MD=1,ND
   12       READ (5,1)  NTHP
   13       READ (5,12) RG,RI
   14       DG=2.*RG
   15       READ (5,14) ZE,ZA,ZC,PSI
   16       READ (5,12) THETA,CDWK
   17       READ (5,1) NQ
   18       READ (5,12) QI,DQ
   19       IF (NTHP-1) 35,31,35
   20    35 IF (NTHP-2) 33,32,33
   21    31 READ (5,13) RF,C,EPSIL
   22       READ (5,12) AREA,PERI
   23       RE=2.*AREA/PERI
   24       GO TO 34
   25    32 READ (5,13) GRVN,WIDTH, DEPTH
   26       RE=WIDTH
   27       GO TO 34
   28    33 READ (5,13) GRVN,WIDTH, DEPTH
   29       READ (5,13) AREA ,PERI
   30       RE=2.*AREA/PERI
   31    34 READ (5,1) NP
   32    21 FORMAT (//72H          ZE                ZA                ZC
             1PSI              THETA)
   33       WRITE (6,21)
   34       WRITE (6,15) ZE,ZA,ZC,PSI,THETA
   35       DO 102 MP=1,NP
   36       READ (5,13) TSAT,PSAT,GRF
   37       READ (5,14) DENF,VSF,CDF,SFT
   38       READ (5,13) HFG,DENG,VSG
   39       DPC=2.*SFT*COS(THETA)/RF
   40       DPS=DENF*GRF*(ZE+ZA+ZC)*SIN(PSI)
   41       IF (NTHP-1) 45,41,45
   42    45 IF (NTHP-2) 43,42,43
   43    41 DPF=C*VSF*(ZE+2.*ZA+ZC)/(2.*3.14159*DENF*HFG*EPSIL*RF*RF)
   44       DPF=DPF/(RI*RI-RG*RG)
   45       GO TO 44
   46    42 DPF=9.*VSF*(WIDTH**2+4.*DEPTH**2)*(ZE+2.*ZA+ZC)
   47       DPF=DPF/(5.*GRVN*DENF*HFG*(WIDTH**3)*(DEPTH**3))
   48       GO TO 44
   49    43 DPF=36.*VSF*(WIDTH**2+DEPTH**2)*(ZE+2.*ZA+ZC)
   50       DPF=DPF/(5.*GRVN*DENF*HFG*(WIDTH**3)*(DEPTH**3))
   51    44 DPG2=32./(3.14159*3.14159*DENG*HFG*HFG*DG**4)
   52       DPGX=4.*VSG/(3.14159*DENG*HFG*DG**4)
   53       DO 103 M=1,5
   54       IF (M-1) 52,51,52
   55    51 DPG1=DPGX*(21.*ZE+32.*ZA)
   56       GO TO 53
   57    52 DNM=EXP(0.8*ALOG(4.7+QWL/(3.14159*HFG*ZE*VSG)))
```

```
      DNM=0.0481+0.0494/DNM
      DPG1=DPGX*(ZE/DNM+32.*ZA)
   53 IF (DPS-DPC) 61,60,60
   60 QWL=0
      GO TO 103
   61 AQ=DPG2
      BQ=(DPF+DPG1)/2.
      CQ=DPS-DPC
  103 QWL=(-BQ+SQRT(BQ*BQ-AQ*CQ))/AQ
      IQ=NQ+1
      DO 104 MQ=1,IQ
      IF (MQ-1) 72,71,72
   71 Q=QWL
      GO TO 73
   72 Q=Q+DQ
   73 DTGE=EXP(0.8*ALOG(4.7+Q/(3.14159*ZE*HFG*VSG)))
      DTGE=2.*Q*ZE*VSG/(3.14159*DENG*(DG**4)*(0.0481+0.0494/DTGE)*HFG)
      DTGA=128.*VSG*Q*ZA/(3.14159*DENG*(DG**4)*HFG)
      DTGC=32.*Q*Q/(3.14159*3.14159*DENG*HFG*HFG*(DG**4))
      DTGE=TSAT*DTGE/(DENG*HFG)
      DTGA=TSAT*DTGA/(DENG*HFG)
      DTGC=TSAT*DTGC/(DENG*HFG)
      IF (NTHP-1) 82,81,82
   81 CDE=CDF*(CDF+CDWK-(1.-EPSIL)*(CDF-CDWK))/(CDF+CDWK+(1.-EPSIL)*(CDF
     1-CDWK))
      DTWE=Q*(RI-RG)/(3.14159*CDE*ZE*(RI+RG))
      DTWC=Q*(RI-RG)/(3.14159*CDE*ZC*(RI+RG))
      GO TO 83
   82 EPP=GRVN*WIDTH/(3.14159*(RI+RG))
      CDE=EPP*CDF+(1.-EPP)*CDWK
      DTWC=Q*(RI-RG)/(3.14159*CDE*ZC*(RI+RG))
      DTWE=(EXP(5.4*DEPTH/WIDTH)-EXP(-5.4*DEPTH/WIDTH))/(EXP(5.4*DEPTH
     1/WIDTH)+EXP(-5.4*DEPTH/WIDTH))
      DTWE=0.185*Q*DTWE/(GRVN*ZE*CDF)
   83 TE=TSAT-DTGE+DTWE
      TC=TSAT-2.*DTGE-DTGA-DTGC-DTWC
      DTEC=DTGE+DTGA+DTGC+DTWC+DTWE
   22 FORMAT (//69H      TSAT              QMAX              TE              TC
     1              DT)
      IF (MQ-1) 92,91,92
   23 FORMAT (/53H      Q                 TE                TC                DT)
   91 WRITE (6,22)
      WRITE (6,15) TSAT,Q,TE,TC,DTEC
      WRITE (6,23)
      Q=QI-DQ
      GO TO 93
   92 WRITE (6,14) Q,TE,TC,DTEC
   93 CONTINUE
  104 CONTINUE
  102 CONTINUE
  101 CONTINUE
      CALL EXIT
      STOP
      END
```